Dithienothiophenes at Work: Access to Mechanosensitive Fluorescent Probes, Chalcogen-Bonding Catalysis, and Beyond

---

Strakova, Karolina; Assies, Léa; Goujon, Antoine; Piazzolla, Francesca; Humeniuk, Heorhii; Matile, Stefan

Dithienothiophenes at Work: Access to Mechanosensitive Fluorescent Probes, Chalcogen Bonding Catalysis, and Beyond

Karolina Strakova, Lea Assies, Antoine Goujon, Francesca Piazzolla, Heorhii V. Humeniuk and Stefan Matile*

Department of Organic Chemistry, University of Geneva, Geneva, Switzerland
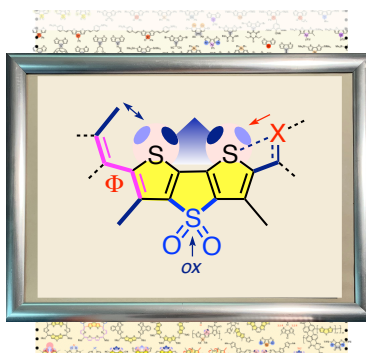
Abstract: In this review, the multifunctionality of dithieno[3,2-*b*:2',3'-*d*]thiophenes (DTTs) is covered comprehensively. This is of interest because all involved research is very recent, emphasizes timely topics such as mechanochemistry for bioimaging or chalcogen bonds for catalysis and solar cells, and because the newly emerging privileged scaffold is embedded in an inspiring structural space. At the beginning, DTTs are introduced with regard to nomenclature, constitutional isomers and optoelectronic properties. The structural space around DTTs is mapped out next with regard to heteroatom substitution in bridge and core, covering much of the periodic table, eccentric heteroatom doping and bridge expansions. After a brief summary of synthetic approaches to the DTT scaffold, chalcogen bonds are introduced as, together with redox switching and turn-on fluorescence, one of the three conceptual foundations of most multifunctionality. Realized functions cover anion binding, transport (ion carriers, ion channels), catalysis, and the first fluorescent probes to image physical forces in living cells. The appearance of DTTs in many other photosystems covers push-pull systems for non-linear optics and dye-

sensitized solar cells, DTT polymers in light-emitting diodes, organic field-effect transistors and organic photovoltaics, DTT self-assembly and templated assembly into thin films and fluorescent fibers, also within cells, and the integration of DTTs into photochromes and biaromatics that violate the Hückel rules.

CONTENTS

1. INTRODUCTION

The emergence of dithieno[3,2-*b*:2',3'-*d*]thiophenes (DTTs) as a privileged scaffold in functional supramolecular chemistry can be traced back to a report from the Barbarella group in 2001.[1] This *Chem. Mater.* paper reports that the oxidation of dithienothiophene DTT **1** over DTTO **2** to DTTO2 **3** generates bright blue fluorescence, both in solution and in the solid (Figure 1). At that time, the reversible oxidation of sulfides into sulfoxides and sulfones was already recognized as a universal, most convenient redox switch.[2–5] Interestingly, with DTTs, reversibility, that is the existence of a redox switch has never been clearly explored because the reduction of DTTO2 **3** was of little interest. Closely related endocyclic "sulfones" have been reduced back to sulfides.[6,7] Quick tests made just for this introduction confirm that treatment of DTTO2 **3** with DIBAL (~6 eq) in toluene for 16 h, warming from 0 ºC to room temperature, affords DTT **1** in 72% yield, whereas excess DIBAL and LiAlH$_4$ also remove the sulfur bridge and yield the respective dithiophene among other products (not shown).
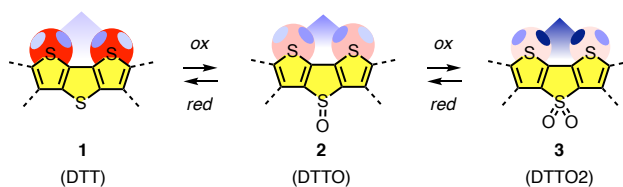
Figure 1. Oxidation of DTT **1** to DTTO **2** and DTTO2 **3** generates bright fluorescence and deep σ holes (blue circles) with a central focal point (blue triangles).

The combination of sulfur redox switches with the emergence of bright blue fluorescence did not attract immediate scientific attention. Some applications as fluorescent probes and photosystems naturally followed, including organic solar cells. However, it took more than fourteen years until the functional relevance of the σ holes on the two endocyclic sulfurs, particularly their deepening during DTT oxidation, was fully appreciated.[8] With this second key characteristic understood, multifunctionality unfolded rapidly: Anion binding, catalysts that operate with unorthodox chalcogen bonds, anion transport covering not only carriers but also synthetic ion channels, or mechanosensitive fluorescent probes to image physical forces in living cells. This emerging multifunctionality of the DTT scaffold, i.e., DTTs at work, in action, will be reviewed comprehensively in the following. The material will be embedded into a broader picture of the DTT scaffold that puts this emerging multifunctionality into the context of a quite remarkable structural diversity, a very well-developed organic synthesis, and an extensive appearance as component in organic materials such as organic photovoltaics (OPVs), organic field-effect transistors (OFETs) and light-emitting diodes (LEDs). These three topics have already been reviewed comprehensively from different points of view, particularly by the groups of Ozturk and Bäuerle, and will thus be treated more generally.[9–18]

2. DITHIENOTHIOPHENES

Dithieno[3,2-*b*:2',3'-*d*]thiophenes **1** can be considered as 2,2'-bithiophenes **4** that are bridged with a sulfur atom to produce central thiophene ring between the two originals in the periphery, with the central sulfur pointing in the opposite direction of the two peripheral ones (Figure 2). Alternatively, it can be considered as a thieno[3,2-*b*]thiophene **5** with a thiophene added or a thieno[2',3':4,5]thieno[3,2-*b*]thieno[2,3-*d*]thiophene **6** with one removed.

Among the five constitutional isomers of [3,2-*b*:2',3'-*d*]-DTT **1**, [3,2-*b*:3',4'-*d*]-DTT **7** is the closest relative, followed by the equally related [3,4-*b*:3',4'-*d*]-DTT **8** and [2,3-*b*:2',3'-*d*]-DTT **9**. More distant is [2,3-*b*:3',4'-*d*]-DTT **10**, and [2,3- *b*:3',2'-*d*]-DTT **11** with all sulfurs on the same side is at the other extreme.

Both 2,2'-DTT dimers **12** and 3,3'-DTTs dimers **13** have been reported.[19,20] Cross conjugated, the absorption maximum of 3,3'-dimer **13** is blue shifted (310 vs 390 nm). Possible oligomerization also includes mixed 2,3'-fusion or another sulfur bridge converting **12** into heptacycle **14**.[21] The synthesis of **14** has been realized with four solubilizing alkyl chains in the periphery.

In solution, DTTs such as **1** absorb broadly around 300 nm (Figure 3).[22] With a quantum yield <1%, fluorescence is barely detectable. Oxidation to DTT *S,S*-dioxides (DTTO2) such as **3** shifts the absorption to around 350 nm and produces the bright blue fluorescence mentioned in the introduction (Figures 3, 4).[1] For the pure scaffold **3**, emission in solution is maximal around 450 nm, the quantum yield in solution is 75%. Even as a powder, a quantum yield of 12% remains. Already in the original Barbarella paper, significant tolerance of this bright fluorescence toward structural elaboration is noted. Methyl groups in **15** do not reduce quantum yields. Sulfoxides in DTTO **16** produce red-shifted maxima compared to sulfone bridges in the homologous DTTO2 **15**. Emission intensity is much reduced in solution, but not in the solid. Control **17** with the same three thiophene heterocycles but separated by single bonds is not fluorescent in solution, whereas fluorescence in the solid remains surprisingly high.

Peripheral phenyls in **18** shift absorption and emission to the red without losses in quantum yield. The same is true for peripheral methylthiophenes in **19**. This modification is interesting because the four methyls around the two bonds connecting to the DTTO2

Figure 2. Structural space around the privileged scaffold **1**.

core twist the peripheral thiophenes out of co-planarity without complete loss of conjugation, as can be seen from the red shifts (*vide infra*). Increasing chromophore planarization upon removal of the methyls in the peripheral thiophenes produces additional red shifts for a complete series of sulfone, sulfoxide and sulfide bridges in **20**–**22**.[23] Whereas the LUMO energy of **22** was too high to be detected by cyclic voltammetry (CV), a gradual decrease to −3.08 eV and −3.17 eV was observed with increasingly electron withdrawing sulfoxide and sulfone bridges in **21** and **20**. Addition of another thiophene at both termini produces additional red shifts and lowering of the LUMO levels in the series **23**–**25**, culminating in −3.32 eV for DTTO2 **23**.

Peripheral imide acceptors proved most effective to further lower the LUMO energies.[24] Already with sulfur bridges in DTT **26**, CV results gave −3.82 eV against −5.10 eV for Fc+/Fc. Withdrawing perfluorinated alkyl substituents in **27** further lowered the LUMO level without much changes in spectroscopic properties. The LUMO levels of DTT **28** with two peripheral arylimides are at −3.72 eV.[25]

6

Sulfone bridges combined with peripheral imides yield a record –4.04 eV for **29**. Peripheral cyano acceptors are less effective than imides.[8] Measured under identical conditions, dicyano DTTO2 **30** affords –3.70 eV compared to –4.04 eV for **29** (Figures 3, 5). Removal of one cyano acceptor raises the LUMO of **31** to –3.30 eV, a sulfoxide bridge in dicyano DTTO **32** affords –3.20 eV. For comparison, the unsubstituted DTTO2 **33** gives –2.88 eV under these conditions. Contrary to their high Hammett σ_p = +0.77,[26] peripheral sulfone acceptors in DTTO2 **34** are with –3.64 eV slightly less effective than cyano acceptors in DTTO2 **30** ($\sigma_p^+ = \sigma_p = +0.66$).[8] Peripheral aldehyde acceptors appear with –3.42 eV for DTTO2 **35** also less effective than expected from their high value ($\sigma_p^+ = +0.73$, $\sigma_p = +0.42$). This underperformance of aldehyde and sulfone acceptors is well explained with intramolecular 1,4 O-S chalcogen bonds that reinject the electron density removed from the scaffold (*vide infra*).
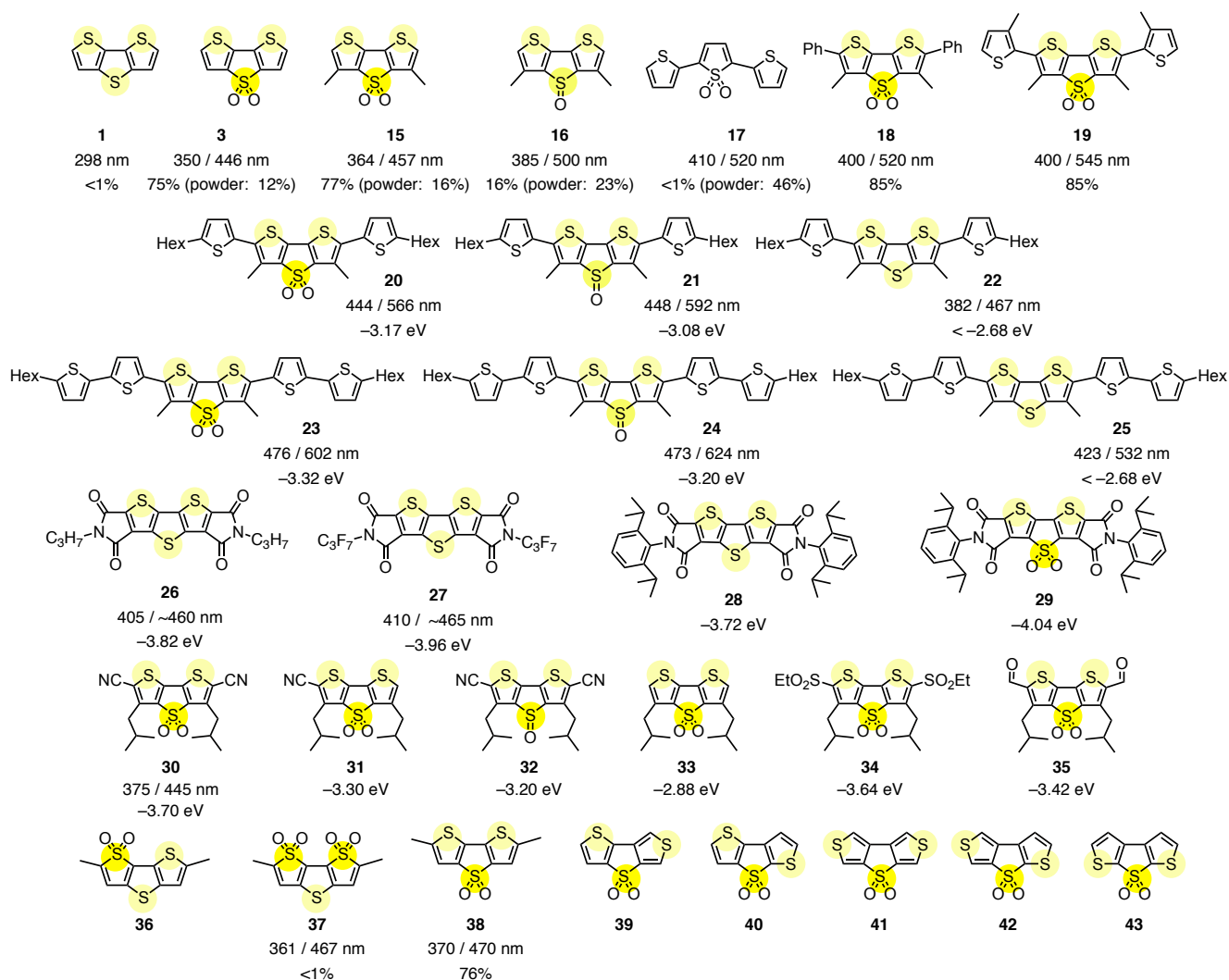
Figure 3. Structural space covered with DTTs, with indication of pertinent absorption / emission maxima (in nm), fluorescence quantum yields in solution (in %), and LUMO energies (in eV, against –5.1 eV for Fc$^+$/Fc, if available). All other data are as reported in the originals with the only intention to highlight relevant trends, different conditions have to be considered for comparison between different reports.
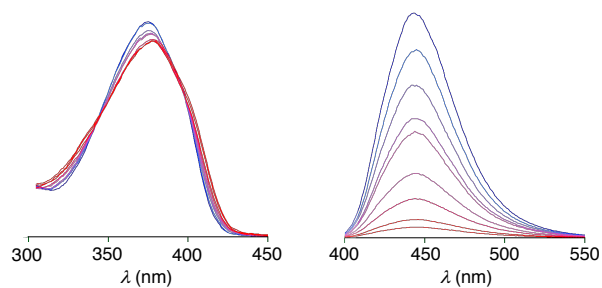
Figure 4. Representative absorption (left) and emission spectra (right) of DTTs, showing the response of DTTO2 **30** to the presence of chloride anions in THF (TBACl, from blue to red with increasing concentration). Adapted with permission from ref. 8. Copyright 2016 American Chemical Society.
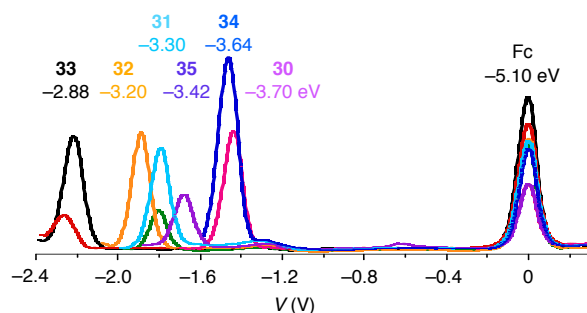
Figure 5. Differential pulse voltammograms of representative DTTs with Fc^+/Fc as internal standard to calibrate LUMO energies against –5.10 eV. Adapted with permission from ref. 8. Copyright 2016 American Chemical Society.

The selective oxidation of one and two of the intrinsically disfavored sulfurs in the core rather than in the bridge has become possible recently.[27] Both DTTO2 **36** and DTTO4 **37** are not fluorescent. Control **38** confirms that this loss of fluorescence is not caused by the methyl groups next to the sulfurs in the DTT core. Oxidized versions of most constitutional isomers of [3,2-*b*:2',3'-*d*] DTT **1** have been reported, examples **39–43** already in the initial synthesis reports from the Janssen group in 1971.[22,28] More developed DTT structures will be introduced later on, together with their functions.

Absorption and emission spectra of ordinary DTTs are usually without further interest, without resolved vibrational finestructures and with little solvatochromism (Figure 4). The same is true for CV and differential pulse voltammetry (DPV, Figure 5).[23] All LUMO energies obtained from these voltammograms are generally high, DTTs are easier oxidized than reduced, transport holes better than electrons (*vide infra*). The energy levels naturally descend from DTT to DTTO and DTTO2. However, also decorated with many acceptors, the record low is –4.02 eV for diimide **29**,[25] a value that naphthalenedimides (NDIs) or fullerenes already reach without any additional acceptors.[2,29]

3. STRUCTURAL SPACE

The substitution of the sulfur heteroatoms in the DTT bridge (Y) and the DTT core (X) is attracting much attention (Figure 6). By now, bridge permutations cover most chalcogen, pnictogen and tetrel atoms. Many, overall a bit more focused examples also exist on core permutations. Eccentric heteroatom doping focuses mostly on thiazoles with nitrogens in position Z. After covering these three general topics, chapter 3 will close with the few examples on bridge expansion. An overview of heteroatom permutations is of particular interest in the context of this review because a projection of the emerging multifunctionality of DTTs into the vast structural space available is likely to stimulate much future progress.
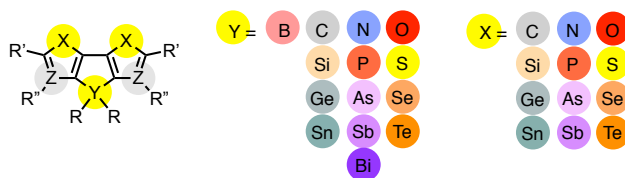
Figure 6. Classification of heteroatom modifications in the DTT scaffold (X = Y = S, Z = C) as bridge (Y), core (X) and eccentric substitution (Z).

3.1. BRIDGE SUBSTITUTION

The emergence of DTTs as a privileged multifunctional scaffold chiefly originates from access to a combination of bright fluorescence, strong chalcogen bonds and redox switching (*vide infra*). It was thus interesting to see how bridge substitutions influence these three key characteristics. A direct comparison of the brightest bridges has been reported in 2012.[30] The standard is set by DTTO2 **45** with peripheral phenyl groups (Figure 7). Fluorescence emission in solution is at 509 nm, and QY at 90%, and 94% in solid state. The fluorescence lifetime, important for imaging applications, is at τ = 5.7 ns, and the LUMO energy at −3.58 eV under the conditions used. Substitution of the sulfone bridge in **45** by a phenylphosphine oxide produces the highly fluorescent dithieno[3,2-*b*:2',3'-*d*]phosphole oxide **46**. However, compared to the chalcogen bridged **45**, the fluorescence quantum yields decreases significantly to 75% for the pnictogen bridged **46** in solution. Emission red shifts slightly to 529 nm, lifetime increases slightly to 6.0 ns. Significant and interesting is the increase of the LUMO by +0.5 eV. With a quantum yield at 81%, the tetrel bridged **47** remains highly fluorescent, whereas emission shifts slightly to the blue, LUMOs remain very high, and lifetimes, interestingly, decrease strongly. Moving within tetrel bridges from silole **47** to the heavier germole **48**, all worsens except for, if desired, constantly high LUMOs at -3.00 eV. Compared to DTTO2 **45**, quantum yields drop from 90% to 50%, lifetimes from 5.7 ns to 1.3 ns, and emission from 509 nm to 483 nm.

With lowest LUMO and strongest fluorescence, this comparison supports DTTO2 **45** as most promising for function. More specific comparisons within all groups confirm this impression. Heteroatom permutations among chalcogens remain quite poorly explored, although synthetic access to furans[31] and selenophenes[32] has been demonstrated with **49** and **50**, respectively. Contrary to the chalcogen bridges beyond sulfur, the pnictogen series has been explored extensively. Dithieno[3,2-b:2',3'-d]pyrroles (DTPs) have attracted much attention as hole transporting polymers in optoelectronic devices, particularly organic solar cells.[33–41] The substituent on the endocyclic bridge nitrogen strongly affects the LUMO energy. For instance, alkyl substituents place the LUMO of DTP **51** +0.43 eV above the homologous DTTs, whereas aryl substituents add only +0.28 eV to DTP **52**.[33] Both DTPs are not fluorescent. This lack of fluorescence of DTPs contrasts sharply with the bright blue emission from dithieno[3,2-b:2',3'-d]phospholes.[13,14,42–44] Impressive comprehensive studies over more than a decade by the Baumgartner group on dithienophospholes confirm that already the minimalist **53** emits at 415 nm with a quantum yield of 78% (Figure 7). The complementary DTT **1** absorbs at 298 nm without significant fluorescence (Figure 3).

Oxidation of the trivalent phosphorus in phosphole **53** to the pentavalent oxide **54** preserves most fluorescence (Figure 7). This constant fluorescence of phospholes is complementary to the turn-on fluorescence from ≤1% to 75% upon oxidation of DTT **1** to DTTO2 **3** (Figure 3). Phosphorus quaternarization with alkyl halides is interesting because the phosphonium cation in the bridge produces phosphole amphiphiles.[13,43] With tris(dodecyloxy)benzyl tails in **55**, highly fluorescent, thermo- and mechanosensitive liquid crystals and ionic organogels could be obtained. Withdrawing pentafluorophenyl substituents in **56** are most attractive to lower the LUMO level and shift emission significantly to the red without losses in intensity.[44] Peripheral expansion produces more substantial red shifts.[13] In the presence (but not in the absence) of terminal aryl amines, oxidation from P^{III} in **57** to P^V in **58** causes a strong blue shift in emission from 630 nm to 566 nm. This is contrary to red shifts with

45
414 / 509 nm
90% / 5.7 ns (94%)
−3.58 eV

46
419 / 529 nm
75% / 6.0 ns (90%)
−2.95 eV

47
408 / 493 nm
81% / 2.8 ns (86%)
−3.04 eV

48
401 / 483 nm
50% / 1.3 ns (70%)
−3.00 eV

49

50

55
em: 467 nm

56
439 / 539 nm
63%
−2.12 eV (calc,
P(III): −1.51, Ph: −1.31)

51
<2%
+0.43 eV vs DTT

52
<2%
+0.28 eV vs DTT

53
338 / 415 nm
78%

54
346 / 424 nm
69%

57
em: 630 nm

58
em: 566 nm

59
334 / 407 nm
7% (15%)
−2.63 eV

60
435 / 456 nm
25% (7%)
−3.00 eV

61
359, 376 / 635 nm
0.2%

62
355 / 420, 625 nm
<2%
−1.77 eV (calc)

63
356 / 400, 625 nm
<2%
−1.69 eV

64
346, 357 / 622 nm
0.2%

65

66

67

68

69

70

71

72

73

74
22% (79%)

75
90% (83%)

76
em: 533 nm (15%)

77
em: 576 nm (8%)

78

79
356 / 425 nm
69%

80
350 / 409 nm
71%

81
<1% (56%)

82

83
366 / 435 nm
17% (6%)

84
358 / 421 nm
9%

85
360 / 434 nm
80% (49%)

86
552 / - nm
−3.1 eV

13

Figure 7. DTT bridge substitutions, with indication of pertinent absorption / emission maxima (in nm), fluorescence quantum yields in solution (in %) / lifetimes (in ns) (fluorescence quantum yields in the solid state), and LUMO energies (in eV).

terminal amines and with the minimalist **53** or **54**. This fluorescent scaffold has very recently been shown to report on Lewis acidity, through contacts with the phosphole oxygen.[45]

Moving down the pnictogens, the full collection is available, from dithieno[3,2-*b*:2',3'-*d*]arsoles **59–61**[46–48] over dithieno[3,2-*b*:2',3'-*d*]stiboles **62**[49] to dithieno[3,2-*b*:2',3'-*d*]bismoles **63** and **64**.[50] None of them is highly fluorescent, and quantum yields decrease with the atomic mass of the pnictogen, whereas the LUMO levels increase. With the heavier pnictogens, the disappearance of fluorescence around 400 nm is compensated by the appearance of a low-energy phosphorescence band around 630 nm, also in the solid state.

The tetrel series starts with cyclopenta[2,1-*b*;3,4-*d*]dithiophenes (CPTs) **65-73**.[15,51–53] As summarized in previous reviews,[15] CPTs have been studied extensively, particularly with regard to applications as polymers in the materials sciences. They can feature either sp^3 or sp^2 carbon bridges. Many examples exist for both. For tetrahedral bridges, macrocyclic motifs **65** and Bingel fullerenes **66** rank among the most inspiring structures. With planar sp^2 bridges, carbonyl groups **67** are most interesting to exploit the rich chemistry of this motif. Examples include alkenes connecting to cation-binding crown ethers **68**, hydrazides **69** with redox active quinones, imines **70**, Knoevenagel acceptors **71**, malonates **72** or heterocyclic classics **73**.

Tetrel bridges beyond carbon have all been covered and reviewed.[16,54–56] Dithieno[3,2-b:2',3'-d]silols attract most attention because of their bright fluorescence. Comparison of silol **47** with DTTO2 **45** reveals that the former is slightly inferior with regard to red shift of emission and quantum yield, and clearly less competitive with regard to fluorescence lifetime and LUMO energy. Peripheral extension with

phosphines in **74** reduces fluorescence in solution but not in the solid state, whereas the borane termini in **75** do not interfere. Dimers **76** and trimers **77** show the expected red shifts and decreasing quantum yields.[57] Push-pull systems **78** with strong tetracyanoethylene (TCNE) acceptors provide access to solvatochromism and environmental sensitivity.[58,59] Ethanol vapor can be sensed with the naked eye from the color change from purple (541 nm) to violet (579 nm) of vapor deposited films. Moving from siloles **79** to germole bridges **80**,[60] LUMO levels increase but spectroscopic properties do not change much, including strong fluorescence. Dithienostannols **81** are poorly fluorescent in solution (<1%) and amorphous powders (9%) but emit bright blue light from single crystals (56%).[56]

From a structural point of view, the most distinguishing characteristic of tetrel bridges is access to dimers, oligomers and polymers. In cyclopentadithiophene **82**, two carbon bridges are connected with a double bond. More common and more general are spiro dimerization at tetrahedral bridges. In silol **83**, spiro dimerization strongly reduces the bright fluorescence of the monomers in solution and solid.[61] Germol centered spiro dimers **84** are also not very fluorescent. Higher oligomers include cyclotetragermoxanes **85**, which, depending on peripheral substituents R, can reach remarkably high fluorescence quantum yields of up to 80% in solution.[55]

Boroles are isoelectronic to 4π-electron cyclopentadienyl cations and thus attract much interest to explore antiaromaticity.[62] Contrary to expectations, this antiaromaticity is further enhanced in dithienoborole **86**.[63] The results are characteristics that differ from the rest of the series, particularly a red shifted absorption at 552 nm, resulting in pink color. Further characteristics include the absence of any fluorescence and low reduction potentials.

3.2. CORE SUBSTITUTION

Like heteroatom substitution in the DTT bridge, heteroatom substitution in the DTT core has been explored extensively (Figure 8). In the chalcogen series, phosphorous-, silicon-, and germanium-bridge difuranes **87–89** have been reported.[64] The pnictogen and tetrel bridges stabilize the difuranes by

lowering their LUMOs. The computed LUMO levels are up to +0.5 eV above the ones of the corresponding dithiophenes. They increase from pnictogen to tetrel and from silicon to germanium bridges. Bond length in crystal structures are consistent with reduced aromaticity compared to bridged bithiophenes. Absorption and emission are blue shifted compared to bithiophenes and bright, with quantum yields up to 80% for the silicon bridged **88**.

Diselenothiophenes **90** and the all-selenium analog **91** have been reported as intermediates of the synthesis of higher oligomers.[32] In the pnictogen series, diselenopyrroles **92** and **93** with electron-withdrawing peripheral substituents are of interest for use as electron-transporting material in OFETs.[65] Absorption maxima and LUMO levels are very similar to the ones of the corresponding DTPs.[66] The comprehensive dibromo series of diselenophenes **94–99** gives most red-shifted absorption toward 400 nm for carbon bridged **97**, most red-shifted emission toward 500 nm for silicon- and germanium-bridged **98** and **99**, lowest LUMOs for electron-withdrawing carbon bridges in **96** at –4.38 eV, followed by **97** with –3.60 eV, and highest LUMO for nitrogen bridged **94** at –2.14 eV, all against –5.1 eV for Fc[+]/Fc.

Bridged bipyrroles attract much interest. Among chalcogen bridges, the most relevant thienobipyrrole **100** has been reported first in 1975.[67–69] The oxidation of the sulfide bridge into the sulfone bridge in **101** has been reported much more recently to afford strongly red-shifted absorption maxima.[69] Synthetic access to furo[3,2-*b*:4,5-*d*]bipyrroles **102** is available as well.[70]

3.3. ECCENTRIC SUBSTITUTION AND BRIDGE EXPANSION

The positioning of heteroatoms in the DTT scaffold is not limited to bridge and core. Eccentric heteroatom doping has mainly focused on motifs bisthiazoles with low LUMO levels. The parent thienobisthiazole **103** has been prepared for co-polymerization with diketopyrrolopyrroles and used as low bandgap p-type semiconductor in OFETs.[71] This study covers also the selenium homolog **104** for the same purpose.[71] Pyrrolo[2,3-*d*:5,4-*d'*]bisthiazoles **105** have been explored quite extensively for use in electron transport materials as part of co-polymers or centered between two NDIs.[72–75] Compared to

DTPs such as **51** (Figure 7), the nitrogen bridge in **105** decreases the LUMO levels significantly (–0.8 eV) and shifts the absorption slightly to the red.

Dithiazolophospholes **106** and **107** have been introduced also for use in organic materials and turn out to remain brightly fluorescent.[76] Arsolobis(thiazole)s **108**, however, are weakly fluorescent.[77] *N*-Doping of cyclopentadithiophene **67** leads to carbonyl-bridged 5,5'-dithiazoles **109** with significantly lowered LUMO.[78]

Bridge expansion beyond single-carbon bridges further widens the chemical space around DTTs. The most obvious bridge expansion affords benzodithiophenes (BDPs) **110**. The bridging benzene lowers HOMO and LUMO. Access to ordered films and high hole mobilities identifies BDP polymers or co-polymers as interesting components of OPVs.[79–81] Substituents on the carbon bridge have been widely varied, from simple solubilizing alkyls and diketo bridges in **111** over various aromatics up to benzocarborano[2,1-*b*:3,4-*b*']dithiophenes.[82] Core substitution within the chalcogen series leads to the very well known benzodifurans **112**.[83] The same substitution in the dione bridged series leads to **113**, and selenium cores afford the corresponding **114** and **115** (nitrogen substituents exist as well).[78,84]

Eccentric heteroatom doping of benzodithiophenes **110** affords benzobisthiazoles **116**.[85] Conversion into the thiazolium salts **117** lowers LUMO levels and removes all fluorescence. The combination of dicarbonyl bridges with eccentric heteroatom doping is realized in 5,5'-dithiazole **118**.[78] Extension of the benzobisthiazole series **116** within the chalcogens leads to benzodiselenazole **119**.[86] The addition of electron withdrawing cyano substituents in the bridge of **120** and the installation of peripheral sulfur redox switches provides access to sulfoxides **121** and sulfones **122**.[86] As an alternative approach to low LUMOs, the injection of positive charges on the eccentric nitrogens in benzodiselenazole **123** by alkylation has been considered.[87] In this series, the interest in lower LUMO levels was not for material applications but to deepen σ holes in the core for applications in catalysis (see below).[86,87]

87
315 / 455 nm
46%, −1.46 eV (calc)

88
338 / 420 nm
80%, −0.96 eV (calc)

89
336 / 400 nm
30%, −0.84 eV (calc)

90

91

92
596 nm
−4.61 eV

93
547 nm
−4.41 eV

94
326 / 368 nm
−2.14 eV

95

96
305 / 420 nm
−4.38 eV

97
389 / 424 nm
−3.60 eV

98
374 / 470 nm
−2.84 eV

99
369 / 467
−2.76 eV

100
385 nm

101
420, 441, 465 nm

102

103

104

105
305 nm

106
344 / 410 nm
(34%)

107
367 / 453 nm

108
327 / 391 nm
(4%)

109

110

111

112

113

114

115

116

117

118

119

120
307 nm / −3.21 eV

121
295 nm / −3.54 eV

122
300 nm / −3.81 eV

123

124
350 nm / −2.29 eV

125
288, 462 /
599 nm
11%, −3.57 eV

126
275, 393 /
458 nm
5%, −3.98 eV

Figure 8. DTT core substitutions, eccentric heteroatom doping and bridge expansions, with indication of pertinent absorption / emission maxima (in nm), fluorescence quantum yields in solution (in %) / lifetimes (in ns) (fluorescence quantum yields in the solid state), and LUMO energies (in eV vs −5.1 eV for Fc⁺/Fc).

18

Further bridge expansion leads to three-atom bridges. Quite extensively studied in this context are bithiopheneimides **124**, introduced in 2008 as n-transporters in conjugated homo- and heteropolymeric OFETs and OPVs.[88,89] The homologous dithienodiketophosphepins **125** combine most attractive spectroscopic properties.[90] With R = *p*-methoxyphenyl (PMP), diketophosphepins **125** emit white light with a QY of 10%. Depending on the wavelength of excitation, two unusual emission maxima at 475 and 600 nm account for the generation of white fluorescence, the former, perhaps, originating from π-π* transition, the latter, perhaps, from intramolecular charge transfer from the triazole donors toward the diketophosphepin acceptors (Figure 9). Increasing red shifts of the absorption maxima with increasingly donating substituents R could possibly support this interpretation. Computational studies also agree with the existence of this push-pull system. The interpretation of solvent-dependent ratiometric emission with twisted conformations in the ground state remains to be confirmed. Exclusive emission at high energy in methanol has been proposed to possibly originate from hydrogen bonding to the triazoles. The low-energy emission could thus perhaps originate from planarization mediated by 1,4 N-S chalcogen bonds. If confirmed, this interpretation could be attractive for mechanosensing applications because, contrary to the more common deplanarization, planarization in the excited state would be quite unusual (*vide infra*). In bent rather than twisted systems, it has been shown to afford ratiometrically-encoded mechanosensitive white emission.[91–93] With mesogenic substituents R in **125**, red, orange-fluorescent gels are obtained. Consistent with a twisted push-pull fluorophore as operational system, all interesting spectroscopic properties disappear upon injection of positive charges into the peripheral triazoles in **126**.[94]

Taken together, this outline of the structural space available around DTTs is made with the intention to put this emerging multifunctional scaffold into context. Many of the lessons learned in the following will be applicable to all the various homologs covered in this chapter. Important are, depending on the function envisioned, access to low LUMO levels for deep σ holes in the core, and bright fluorescence.
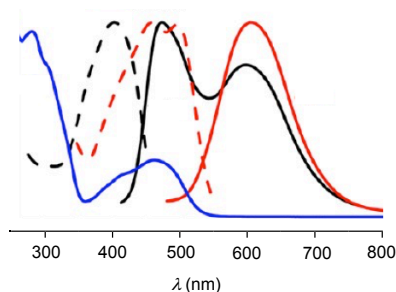
Figure 9. Absorption (blue), excitation (dashed) and emission spectra (solid) of the white-fluorescent dithienodiketophosphepin **125** (R = PMP) in CH$_2$Cl$_2$ with excitation at 400 nm (black) and at 460 nm (red). Adapted with permission from ref. 90. Copyright 2013 American Chemical Society.

4. SYNTHESIS

Today, DTT synthesis is routine.[95] The first synthesis of DTT has been reported by the Janssen group in 1971.[22] The Janssen synthesis starts with the peripheral thiophenes (Scheme 1). Two bromothiophenes **127** are first bridged with a sulfide to give **128**. Then the central thiophene is cyclized into **1** by oxidative, copper mediated C-C bond formation.

The complementary approach from peripheral thiophenes by final bridging of dithiophenes exists as well.[96] Dimethyl thiophene **129**, for instance, is first iodinated. Nickel-mediated coupling of iodothiophenes **130** affords dithiophene **131**. Dibromination gives **132**, which is bridged with (PhSO$_2$)$_2$S to yield the tetramethyl DTT target molecule **133**.

More versatile and more elegant is the currently favored route. This synthesis, first reported by the Holmes group[97] and then refined by Zhu and coworkers,[24] starts with the central thiophene. Tetrabromothiophene **134** is first reacted with two aldehydes **135**, which are then oxidized to give the respective diketone. Cascade cyclization with two 2-thioacetate ethyl esters **136** affords the DTT scaffold in **137**. Ester hydrolysis followed by decarboxylation yields DTT **1**. Stepwise oxidation to DTTO **2** and DTTO2 **3** is routinely achieved with mCPBA (Figure 1).[9–11,95]

20

Scheme 1. Three General Strategies to Synthesize DTTs.
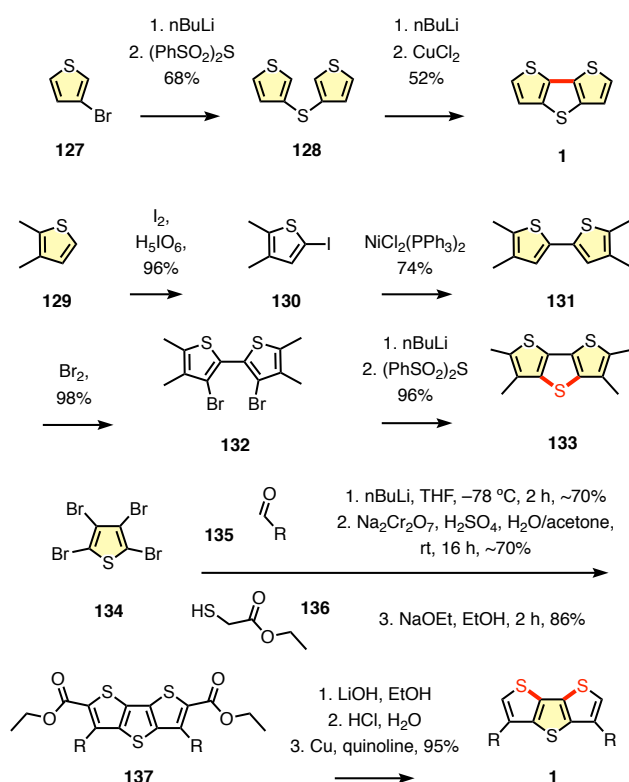
The same methods are used to synthesize bridge-substituted DTT analogs (Scheme 2). Final cross-coupling of two pre-bridged thiophenes is most common with carbon bridges in cyclopentadithiophenes.[15] The carbonyl-bridged tricycle **67**, for example, is prepared from the same bromothiophene **127** used for the analogous synthesis of DTT **1**. Addition to aldehyde **138** followed by oxidation of the resulting alcohol to the ketone and chemoselective iodination gives prebridged **139**, which is then subjected to oxidative Cu coupling to afford the desired CPT **67**.

Most other bridge elements are introduced by final bridging of dibromodithiophenes **140**. Treatment with BuLi followed by the chloride of the respective element directly yields the bridge-substituted DTT such as bismole **64** (Scheme 2). This approach is analogous to the synthesis of DTT **133** by final bridging of dibromo dithiophene **132** with sulfur (Scheme 1).

For oligomerization, the coupling of α-linked isomers is chemically preferred (Scheme 3). Stille coupling is most common today.[20] The original dimer **12** has been prepared from **141** (without silyl group) by Fe-mediated coupling.[19] Access to β-linked dimers **13** is possible from the same monomer **141**.[20] The LDA initiated "halogen dance" affords the β-bromo isomer **142** in excellent yield. Stannylation affords **143** for Stille coupling with **142**. Desilylation of the resulting β dimer with TBAF then yields the final product **13**.

Scheme 2. Representative Syntheses of Bridge-Substituted DTT Analogs.
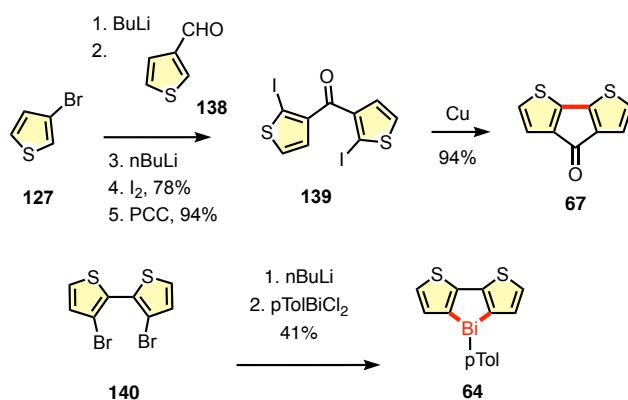
Scheme 3. Representative Synthesis of α- and β-Linked DTT Dimers.
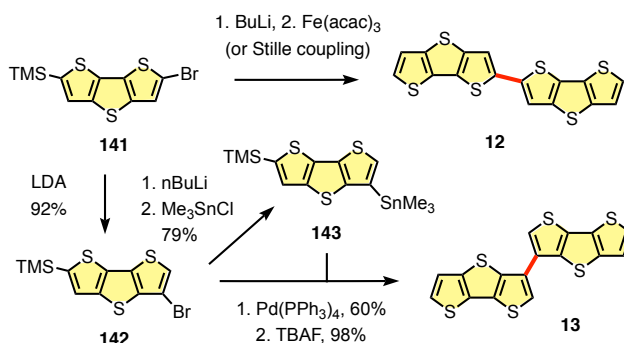
5. CHALCOGEN BONDS

Already in the breakthrough paper from the Barbarella group in 2001, it was observed that DTTO **16** exhibits very close S-O contacts in the crystal (Figure 10A).[1] The bridge oxygen was found precisely
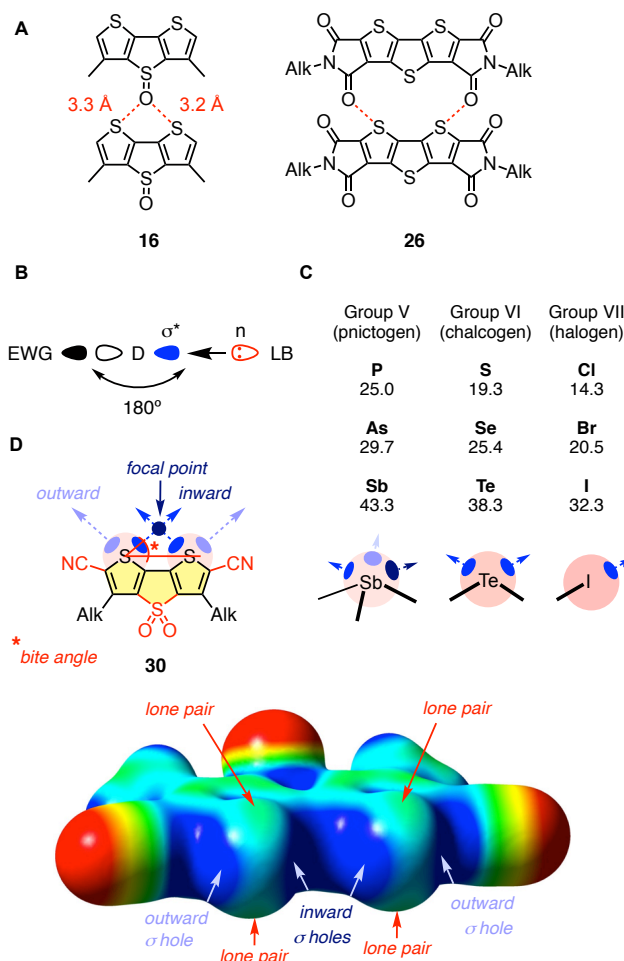
Figure 10. (A) Selected S-O contacts in X-ray structures. (B) σ-Hole interactions between a σ* orbital of donors D and a lone pair n of acceptors LB. (C) σ Holes increase with the polarizability of donors in groups V-VII (MP2 calculations, a.u.). (D) Annotated MEP surface of **30** (red: electron rich, blue: electron poor). Adapted with permission from ref. 8. Copyright 2016 American Chemical Society.

between the two sulfur atoms in the core of the neighboring molecule. Similar observations were reported for several related motifs, for instance the carbonyl-bridged diselenophene **95**.[78]

Intermolecular S-O contacts to the central DTT sulfurs from the outside rather than from the inside occur in the crystals of DTT diimide **26**.[24] These complementary S-O contacts nicely illustrate the presence and location of overall four σ holes on the central DTT sulfurs, two per atom (Figure 10B–D). σ Holes

refer to highly localized areas of high electron deficiency on the molecular electrostatic potential (MEP) surfaces (Figure 10D).[8,12,17,98–117] They can accept electron density from Lewis-basic donors, including anions and lone pairs of neutral donors. The resulting interactions are referred to as halogen, chalcogen, pnictogen and tetrel bonds. Increasing with polarizability of the atom,[98] the interaction energies increase to the left and to the bottom of the periodic table (Figure 10C). Related to the antibonding σ^* orbital, chalcogens can offer two bonds, whereas halogens can produce one, pnictogens three and tetrels four (Figure 10B, C). Compared to hydrogen bonds, chalcogen bonds are much more hydrophobic and directional, i.e., ideal for contacts at high accuracy. At best, they extend co-linearly to the covalent bonds from the opposite side of the donor.

Chalcogen bonds have been extensively studied in the solid and for intramolecular conformational control, particularly in medicinal chemistry.[8,12,17,98–117] The DTT scaffold appeared attractive for chalcogen bonding because, as illustrated in the MEP of **30**, the two inward oriented holes promised powerful acceptor recognition in their focal point (Figures 10C, D).[8] At best, this recognition on the focal point of the inward σ holes could be further controlled through switches at the two outward oriented σ holes.

6. ANION BINDING

For anion binding, the direct chalcogen-bonding counterpart to hydrogen bonding bipyrrole **144** would be 2,2'-bithiophene **4**. However, anion binding to 2,2'-bithiophene **4** is weak because the focal point of the inward σ holes is too close to the scaffold. This mismatch described by a too small bite angle of 23° produces chloride complexes with too small bond angles of 149°, resulting in too long chalcogen bonds up to 3.4 Å. To correct this mismatched topology, both thiophenes have to rotate inward (Figure 11B). This is achieved by the tight, single-atom sulfur bridge in DTTs (Figure 11C). Computational models of chloride complexes of unmodified DTT **15** testify for a perfect bite angle of 45°, adjusted bond angles
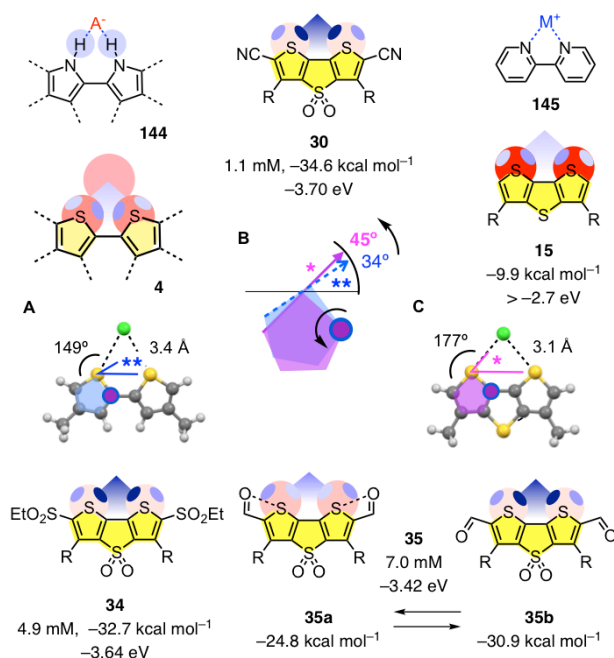
Figure 11. Anion binding with DTTs. (A) Poor chloride (green) recognition above the mismatched focal point of the inward σ holes of the central sulfur atoms in 2,2'-bithiophene **4**, with (**) bite angle, bond angle and bond length. (**B**) Required bite angle adjustment from (**) 34º to (*) 45º by inward rotation of both heterocycles. (C) Anion recognition in the adjusted focal point of the σ holes in DTT **15**, compared to classics such as bipyrrole **144** and bipyridine **145**. Dissociation constants K_D of chloride complexes in THF (in mM) are given in comparison to computed interaction energies (in kcal mol⁻¹) and measured LUMO energies (in eV against –5.1 eV for Fc⁺/Fc).

near 180º, shortened chalcogen bond length below the sum of the VdW radii, and increased interaction energies as a consequence.

Chalcogen bonding in the focal point of their inward σ holes identifies DTTs as a privileged scaffold that is reminiscent of classics such bipyrroles **144** for anion binding by hydrogen bonding as bipyridines **145** for cation binding (Figure 11). The failure of the atom-per-atom analogous bithiophene **4** to perform like bipyrrole **144** nicely illustrates that chalcogen-bond donors are more directional than hydrogen bond donors. Upon bite angle adjustment in DTTs **15**, amplification of this high directionality in the focal

point of two σ holes therefore promises access to high-precision activities in the corresponding functional systems. The computed chloride interaction energies increase from sulfide bridges in **15** to sulfone bridges in **30**, **34** and **35**. On the sulfone level, chloride interaction energies increase from peripheral aldehydes in **35** to sulfones in **34** and cyano acceptors in **30**. This increase corresponds to the decrease of the LUMO levels, i.e., the depth of the σ holes.

Chloride binding in THF can be followed directly by changes in absorption and emission maxima in the presence of increasing concentrations of TBACl (Figure 4).[8] The resulting dissociation constants K_D decrease from **35** with $K_D = 7.0$ mM to **34** with $K_D = 4.9$ mM and **30** with $K_D = 1.1$ mM. The coincidence of this stabilization of the 1:1 complexes with decreasing LUMO levels and increasing interaction energies supports the existence of operational chalcogen bonds.

The peripheral aldehydes in **35** are of particular interest because they could form switchable intramolecular 1,4 O-S chalcogen bonds with the outward σ holes in the DTT core (Figure 11). These outward chalcogen bonds weaken the inward chalcogen bond to the anion in their focal point from −30.9 kcal/mol in **35b** to −24.8 kcal/mol in **35a**. Compared to cyano acceptors in **30** (−3.70 eV) that do not form these competitive outward chalcogen bonds, the LUMO level of **35** is with −3.42 eV indeed rather high. In contrast, chloride binding by **35** ($K_D = 7.0$ mM) is not much weaker than by **30** ($K_D = 1.1$ mM). This strong chloride binding despite high LUMO suggests that without anion, the peripheral aldehydes reinject charge density by chalcogen "back-bonding" in **35a**, whereas upon anion binding, the outward σ holes weaken, the intramolecular chalcogen bonds break and conformer **35b** dominates. This anion-responsive conformational switch on the outward σ holes in the DTT core is most attractive for dynamic adaptive control in functional systems (*vide infra*). Theoretical conformational analysis of 2,5-diamide-thiophene derivatives confirms the corresponding preference for double chalcogen bonding interactions.[118] DTTs were not the first chalcogen-bonding anion hosts,[8] several reports with unrelated systems have appeared previously.[119–121]

Anion binding in the focal point of the inward σ holes of DTTs has been confirmed in computational studies in systematic comparison with phosphorus, arsenic and germanium in the core of analogs **146-148** (Figure 12).[122] Coverage of the full series for sulfide, sulfoxide and sulfone bridges indicates that interaction energies increase with decreasing LUMO levels. Increasing interaction energies with S<P<As<Ge in the core are consistent with the polarizability of these atoms (Figures 10C, 6). For all compounds tested, significant F>Cl>Br>I selectivity sequences were obtained. With hydrogens completing the elements in the core, it is understood that **146-148** are hypothetical molecules. The same accounts for computational studies that suggest strengthened anion binding by nitrogens added next to the sulfurs in the DTT scaffold.[123]

3	**146** (HM)	**147** (HM)	**148** (HM)
−42.3 kcal mol^{-1}	−50.7 kcal mol^{-1}	−53.9 kcal mol^{-1}	−63.4 kcal mol^{-1}
(n = 2)	(n = 2)	(n = 2)	(n = 2)
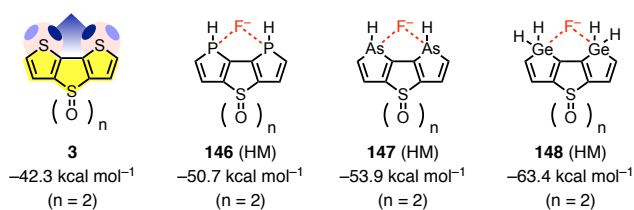
Figure 12. Selected interaction energies in kcal mol^{-1} computed for DTT analogs operating with pnictogen and tetrel bonds (HM = hypothetical molecules).

7. CATALYSIS

Anion stabilization in the ground state obviously implies that anionic transition states can also be stabilized in the focal point of the inward σ holes in the DTT core. To elaborate on DTTs as catalysts, the transfer hydrogenation of quinolines **149** with Hantzsch ester **150** as hydride donor was selected as model reaction, affording amines **151** and pyridine **152** as products (Figure 13).[25] Transfer hydrogenation of imines **153** to amines **154** was added for comparison. Computational studies confirm recognition of nitrogen lone pairs in aromatic heterocycles as in substrate **149** in the focal point of the inward σ holes of DTTO2 **30**. Rate enhancements up to k_{cat}/k_{uncat} = 1290 for DTTO2 diimide **29** were found (Figure 14).

Increasing rate enhancements with increasing anion binding energies support the existence of operational chalcogen bonds in catalysis. This first observation of intermolecular catalysis with chalcogen bonds realized with the DTT scaffold was quickly followed by other examples, extending also to pnictogen bonds.[124–127] Catalysis with halogen bonds and covalent conformational control by chalcogen bonds during catalysis has been explored previously in several examples.[103,128,129]
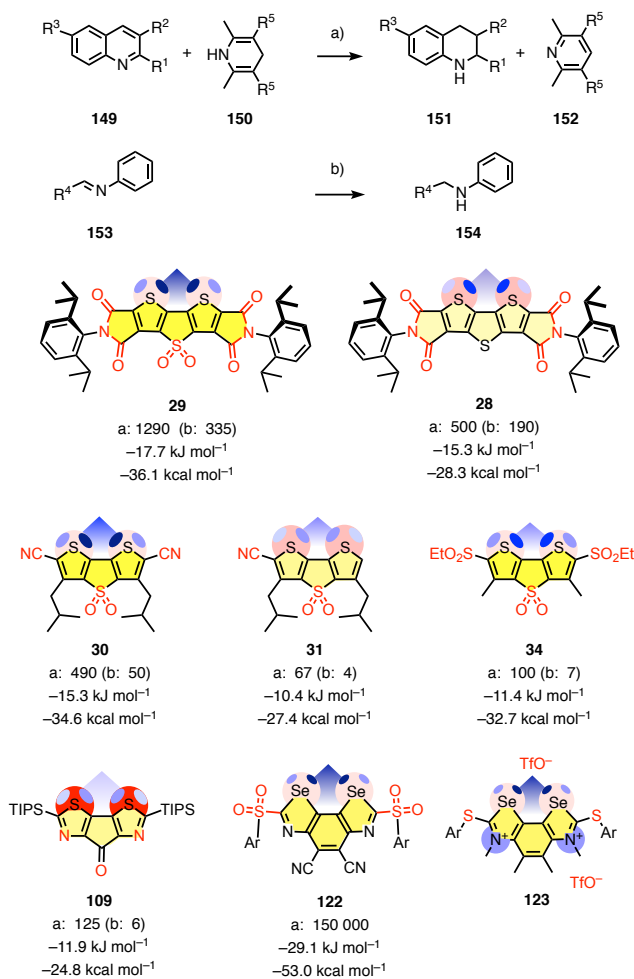
Figure 13. Catalysis with DTTs. Rate enhancements measured for the transfer hydrogenation of a) quinolines **149** ($R^1 = R^2 = R^3 = H$) and (in parenthesis, b) imines **153**, $R^4 = Ph$) with Hantzsch ester **150** ($R^5 = COOEt$) in the presence of different catalysts, with measured transition-state stabilization $\Delta\Delta G^{\ddagger}$ in kJ mol^{-1} against computed chloride-binding energies in kcal mol^{-1}.
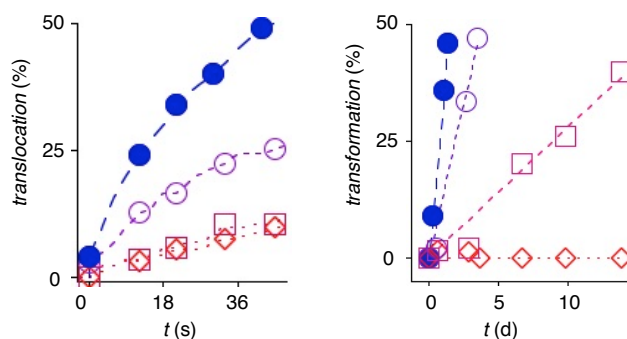
Figure 14. Left: Anion transport across lipid bilayer membranes mediated by DTTO2 **30** (●) and **33** (○) and the redox-switched DTTO (□) and DTT controls (◇). Right: Formation of product **151** from hydride acceptor **149** and hydride donor **150** without (◇) and with 30 mol% catalyst **29** (●), **30** (○) and **34** (□).

The replacement of sulfur with single-carbon bridges together with eccentric nitrogen acceptors as in **109** gives rate enhancements in the range expected from anion-binding energies. Substitution of the central sulfurs in DTT by the more polarizable seleniums was likely to boost catalytic activity.[86] However, placed into the DTT scaffold as in **90** (Figure 8), the longer Se-C bonds were predicted to increase the bite angle and thus move the focal point of the inward σ holes on the central chalcogens away from the scaffold. The resulting mismatch for chalcogen-bond formation was expected to reduce anion binding and catalysis. To readjust the focal point, molecular models suggested to expand the bridge from one to two atoms. The resulting benzodiselenazoles, a new scaffold, gave the expected activities up to k_{cat}/k_{uncat} = 150 000 for **122**, a catalyst equipped with eccentric nitrogens and peripheral sulfone and cyano acceptors. The injection of positive charges by alkylation of the endocyclic nitrogens in **123** was explored as alternative strategy to deepen the σ holes on the Se donors.[87] Crystal structures show one of the two triflate counterions in the focal point of the inward σ holes on the central selenium donors, thus supporting that catalysis still occurs by chalcogen bonding and not by ion pairing.

8. ANION TRANSPORT

Experimental support for DTTs as privileged scaffold for anion binding in the focal point of the inward σ holes invited not only for applications to catalysis but also for anion transport. Anion transport along membrane spanning scaffolds has been achieved for hydrogen bonds,[130] C-H anion interactions,[131] ion pairing,[132] anion-π interactions[133] and halogen bonds.[134] Trimers **155** expand this series to anion transport with chalcogen bonds (Figure 15).[135]

In **155**, three DTTs with deep σ holes are aligned to offer a chalcogen-bonding cascade across the hydrophobic core of lipid bilayer membranes. Irregular single-channel currents are observed in conductance experiments, supporting the self-assembly of amphiphiles **155** into dynamic bundles. A submicromolar EC_{50} = 280 nM is consistent with the formation of synthetic ion channels (EC_{50} = the effective concentration needed to reach 50% of maximal activity). This EC_{50} is more than one order of magnitude below controls **156-158** and **30**. These include trimers without a transmembrane chain of deep σ holes (**156**, EC_{50} = 3.5 μM), shortened dimers (**157**, EC_{50} = 4.0 μM), and more twisted dimers with isobutyl groups along the scaffold (**158**, EC_{50} = 7.8 μM).

These amphiphilic oligomer controls are also less active than the best monomeric anion carrier **30** (EC_{50} = 1.9 μM).[8] Contrary to the immobile, membrane-spanning channels **155**, ion carriers **30** shuttle across the bilayer membranes together with the bound anion they transport. In carrier **30**, the σ holes for anion binding are deepened by sulfone and cyano acceptors in bridge and periphery, respectively. Activities decrease with decreasing depth of the σ holes. Examples include DTTO2 **31** with only one cyano acceptor (EC_{50} = 7.0 μM), DTTO **32** with a sulfoxide bridge (EC_{50} = 22 μM) and DTTO2 **33** without cyano acceptors (EC_{50} = 9.4 μM, Figures 3, 14. 15). Carrier **30** and channel **149** are the first examples for transmembrane anion transport mediated by chalcogen bonds. Other examples and extension to pnictogen bonds followed.[136]

9. FLUORESCENT PROBES

The potential of DTTO2 as fluorescent probes was pointed out early on in the Barbarella group.[137,138] A small collection of rainbow probes **159-169**, covering the whole visible window, blue to orange fluorescence, was equipped with isocyanates for bioconjugation with amines (Figure 16). Binding to antibodies did not change the optical properties, and photostability was very high.
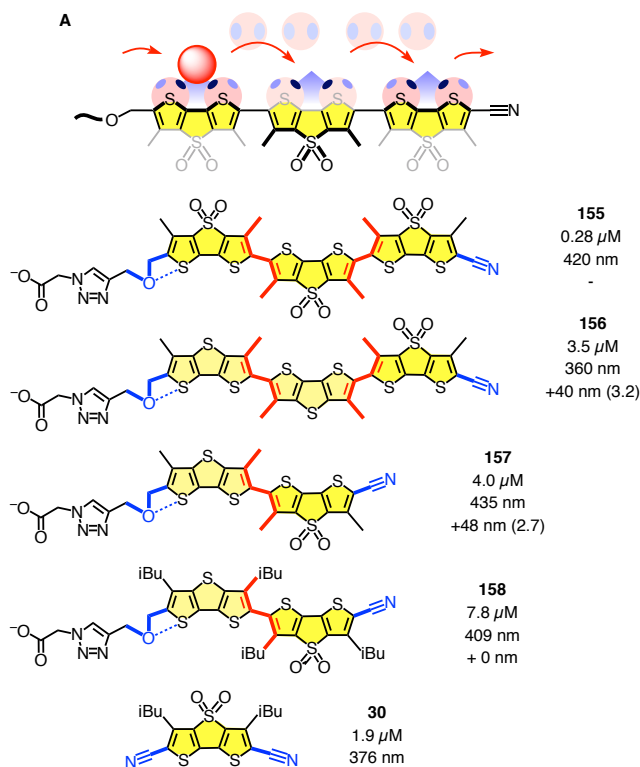
Figure 15. Anion transport across lipid bilayer membranes by (A) anion hopping along chalcogen-bonding cascades occurs in trimer **155** but not in controls **156-158** and the best chalcogen-bonding anion carrier **30**. Given are EC_{50} for transport in vesicles (in μM, the lower the better), absorption maxima in disordered membranes (in nm) and average red shifts of the lowest-energy excitation maxima in ordered membranes (+, in nm).

The imaging of physical forces in action is one of the central challenges in current biology.[139–143] Revealing gravity long ago, Newton's apple illustrates the fundamental nature of the challenge. To do the same for biology called for fundamentally new chemistry. For the development of DTTs as fluorescent force probes, the color change of lobsters during cooking was recognized as a source of inspiration.[144–147] In living lobster, the twisted carotenoid pigment is planarized and polarized until it literally turns blue. Thermal protein denaturation during cooking then allows the pigment to relax into its preferred twisted conformer. Whereas similar combinations of chromophore planarization and polarization in the ground state account for much of the chemistry of vision, particularly color vision,[148,149] fluorescent probes that would operate the same way do not exist. Planarizable push-pull probes were introduced for this purpose.[144] Whereas original proof of principle mechanical planarization in the ground state was readily accessible with twisted push-pull oligothiophenes,[144] compatibility with bioimaging remained beyond reach for long time.[150,151] To solve the two key problems, DTTs were introduced as "fluorescent flippers" because they offer i) large enough surface areas to feel the environment, i.e. mechanosensitivity and ii) sufficient monomer fluorescence to also keep shining when twisted out of conjugation.[152] In the current best probe **157**,[153] the average excitation maximum in liquid-disordered (L_d) membranes is at 435 nm (Figure 17, yellow). Moving from L_d to liquid-ordered (L_o) and solid-ordered (S_o) membranes, this excitation maximum shifts +48 nm to the red, and a shoulder originating from the 0-0 transition in partially resolved vibronic finestructure appears around ~+70 nm (Figure 17, red). At the same time, emission intensity I_{So}/I_{Ld} increases 2.7 times. The insensitivity of the emission maxima to increasing order of the surrounding membrane nicely illustrates that the mode of action of fluorescent flippers differs from other membrane probes operating in the excited state by TICT (molecular rotors), ESIPT, PET, ICT (solvatochromisim), FRET, unbending, and so on.[91,154–167]

	159 438 / 540 nm
	160 368 / 451 nm
	161 401 / 514 nm
	162 425 / 550 nm
	163 422 / 566 nm
	164 383 / 483 nm
	165 404 / 499 nm (>90%)
	166 374 / 454 nm
	167 440 / 600 nm
	168 418 / 552 nm
	169 361 / 463 nm
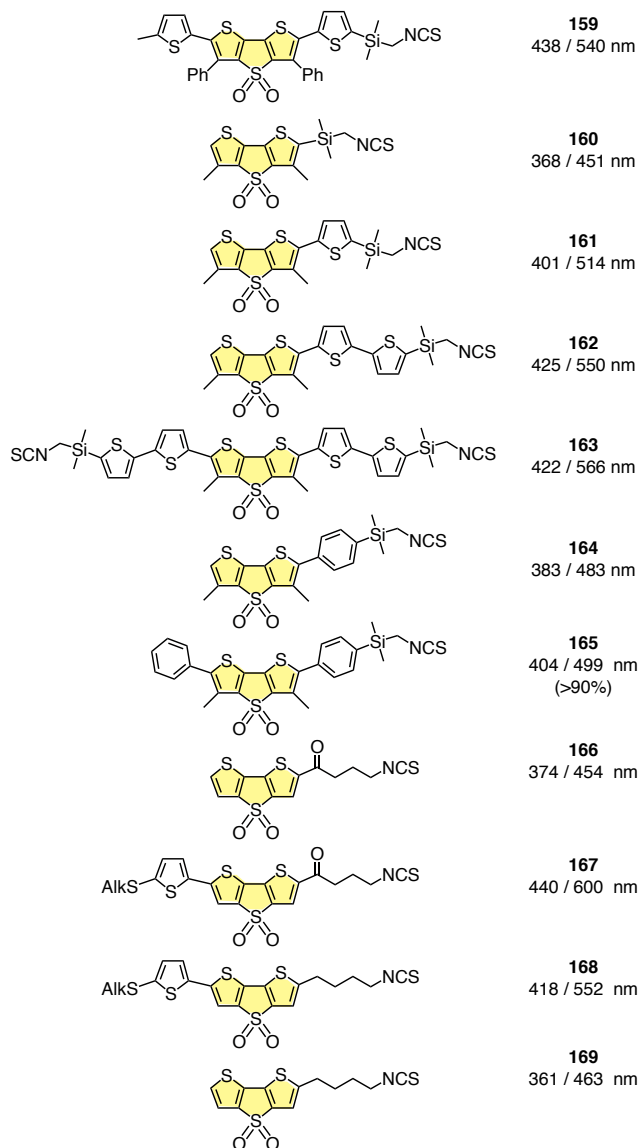
Figure 16. Rainbow probes for bioconjugation from the Barbarella group.

Red-shifted absorption rather than emission was consistent with the planarization of the twisted push-pull DTT dimer **157** with increasing order of the surrounding membrane (Figure 18). In this dimer, the two DTT flippers are twisted out of conjugation by "chalcogen-bond repulsion" between the two methyls and the outward σ holes on the endocyclic sulfur atoms. The push-pull system is built on sulfide donors and sulfone acceptors in the bridges. The latter is supported by a cyano acceptor. An intramolecular chalcogen-bond donor at the other end marks the beginning of the ether-triazole-carboxylate headgroup.

The triazole is essential to prevent elimination (*vide infra*), the carboxylate to deliver the mechanophore to the plasma membrane of cells.

The structure of Flipper-TR™ **157** has been optimized atom by atom. This effort is documented in the design, synthesis and evaluation of analogs **170–183** (Figure 18). With regard to the less explored deplanarization, it was reported that increasing twisting in the leucine flippers **158** destroys all mechanosensitivity in membranes and results in excited-state twisting (TICT) rather than ultrafast planarization (Figure 15).[95] Most reported studies focus on the push-pull system. Substitution of the thenyl ether in **157** by a thenyl ester in **170** shifts the excitation maximum in disordered membranes to the red and, most importantly, mechanosensitivity with regard to both red shift and intensity increase with membrane order (Figure 18).[153] These improvements are roughly independent of the nature of the acceptor on the other terminus, that is cyano in **170** or aldehyde in **171**.
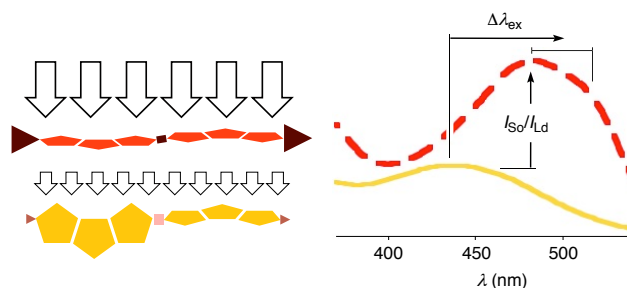
Figure 17. The planarization of twisted push-pull DTT dimers **157** and **170–183** in the ground state with increasing order of lipid bilayer membrane (left) causes a red shift of excitation and an increase in intensity (right).

Despite the superior spectroscopic properties compared to Flipper-TR™ **157**, probes **170** and **171** are not useful for practice because they are chemically unstable and, presumably as a consequence, highly cytotoxic. This chemical instability has been attributed to the elimination of the headgroup, also referred to as a "molecular guillotinylation."[153] Activated by acid (H^+) or base ($B^{(-)}$), headgroup elimination affords the cationic reactive intermediate **184** (Scheme 4). This intermediate is routinely observed as the
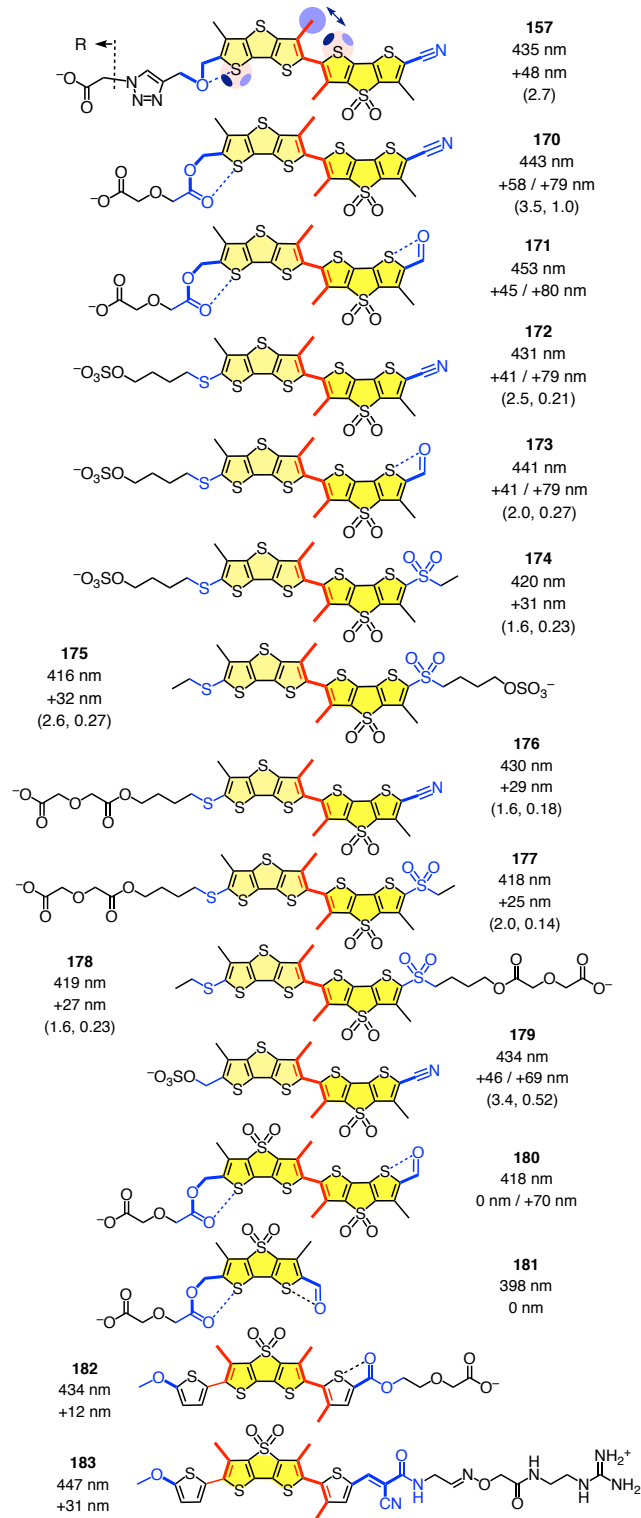
Figure 18. Twisted push-pull DTT dimers **157** and **170–183** with excitation maxima in nm in L_d membranes, shifts from L_d to S_o membranes in + nm (for maxima/bathochromic shoulders), and, in parenthesis, intensities in S_o relative to L_d membranes, followed by, if available, intensities in solution relative to **170**.

35

main peak in mass spectra. The carbocation electrophile then can react with any nucleophile Nu$^{(-)}$ to produce a mixture of products.

Headgroup elimination occurs easily not only with thenyl esters **170** and **171** but also with ethers **185** and carbamates **186** (Scheme 4). In Flipper-TR^{TM} **157**, this process is hindered by the proximal triazole base. Transient protonation will occur there first rather than on the thenyl oxygen to produce the conjugate acid **187** with a p$K_a \sim 1.3$ rather than the oxonium cation **188** with p$K_a < 1.3$.[168] Further protonation of the ether in conjugate acid **189** is then prevented by charge repulsion from the proximal triazolium cation,[132] which increases the acidity of the second cation in **189** to a p$K_a \ll 1.3$ that can be reached only in the presence of an excess of strong acid.

This inhibition of acid-catalyzed leaving group activation by the proximal triazol stabilizes probe **157** sufficiently for use in biology. However, ideally, it would be preferable to attach strong donors directly to the DTT to build a push-pull system as strong as possible and thus maximize the red shifts accessible upon planarization. Whereas these strong donors are required in planarized probes, they are poorly tolerated in twisted form. Without conjugation to the acceptor DTTO2 in the dimer, the injection of more electron density from additional donors makes the donor DTT too rich in electrons and causes rapid oxidation. For instance, model dimer **190** with a methoxy donor on one side and a sulfone acceptor in the other spontaneously decomposes within minutes in the NMR tube under ambient conditions (Figure 19).[169]

To address this dilemma with terminal donors – needed in planar but incompatible with twisted conformation –, the concept of turn-on sulfide donors was introduced (Figure 19A, blue).[169] Attached to electron-rich aromatics, sulfides act as weak acceptors, as demonstrated by the positive Hammett σ_p = +0.03.[26] Attached to electron-poor aromatics, sulfides transform into strong donors, as demonstrated by the strongly negative Hammett $\sigma_p^+ = -0.60$. For comparison, methoxy donors are at $\sigma_p = -0.27$, roughly independent of the electron density in the aromatic ring. Indeed, in sharp contrast to the fragile dimer

Scheme 4. Headgroup elimination in fluorescent force probes.
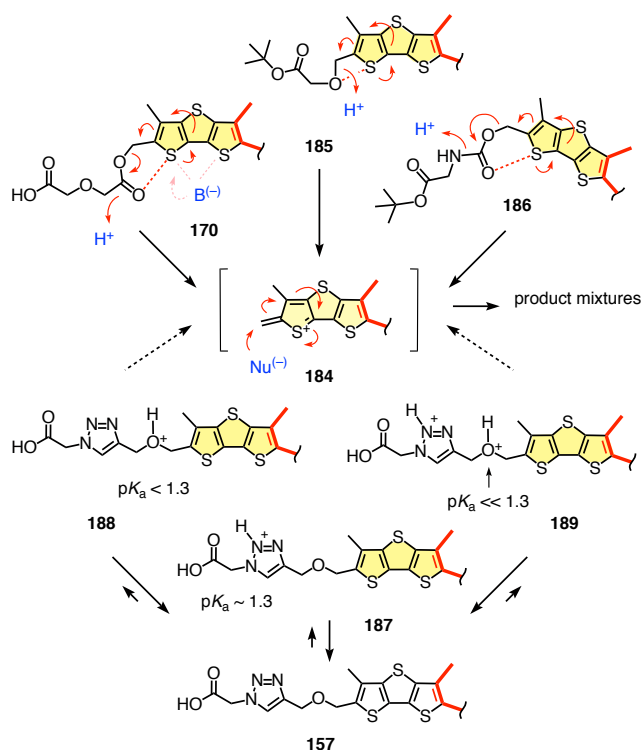
190 with a methoxy donor, dimer **191** with a sulfide donor instead is perfectly stable under ambient conditions. This "all-sulfur" dimer **191** shows a blue-shifted absorption at 403 nm. This blue shift is consistent with the terminal sulfide acting as an acceptor, reducing the push-pull system and increasing the twist. A smaller blue shift in emission compared to excitation is consistent with conversion of the sulfide acceptor into a sulfide donor. The result is a maximal Stokes shift of 9300 cm^{-1} for **191** with a turn-on sulfide donor compared to 8700 cm^{-1} for **190** with permanent methoxy donors, promising maximal mechanosensitivity in response to planarization in the ground state. Originating from turn-on sulfide donors, the same attractive trends occur naturally also with cyano rather than sulfone acceptors in **192** and **193**. Time-resolved emission spectra during spontaneous ultrafast planarization from the Franck-Condon to the first excited state is faster with permanent methoxy ($\tau = 0.45$ ps) than with turn-on sulfide donors ($\tau = 1.5$ ps, Figure 19B), and the latter gives higher quantum yields up to 33%. The existence of
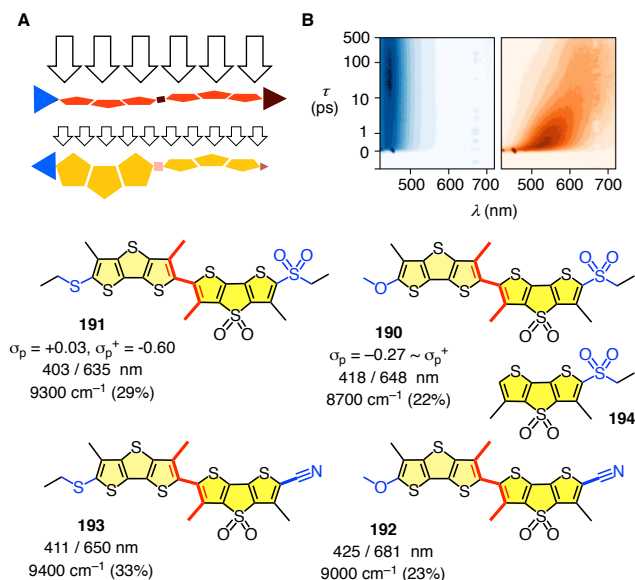
Figure 19. (A) The concept of turn-on sulfide donors to tackle the dilemma of terminal donors in fluorescent force probes: They act as acceptors in deplanarized conformers and convert into donors only upon planarization (blue), with (B) time-resolved emission spectra of **191** (orange) against monomeric control **194** (blue). For model systems **190-193**, indicated are pertinent Hammett σ_p and σ_p^+, excitation / emission maxima in nm, Stokes shifts in cm^{-1} and fluorescent quantum yields in solution in parenthesis. Adapted with permission from ref. 169. Copyright 2015 American Chemical Society.

ultrafast excited-state planarization of **190** and **191** was supported by mechanosensitive kinetics and the absence of any planarization with monomer **194** (Figure 19B).

This promising result with turn-on sulfide models **191** and **193** failed to improve properties in lipid bilayer membrane.[170] The main problem is brightness. Compared to flipper **170** with intramolecular 1,6 S-O chalcogen bonds ($I/I_0 = 1.0$), turn-on sulfide donors in **172** reduce fluorescence intensity to $I/I_0 = 0.21$ (Figure 18). Intensity increases upon ground-state planarization, i.e., mechanosensitivity, suffer similarly. Even the red shift of the excitation maxima decreases slightly. Substitution of the cyano acceptor in **172** by aldehydes in **173** and sulfones in **174** does not improve performance. With sulfone

acceptors, it was possible to move the negatively charged sulfonate headgroup from the donor side in **174** to the acceptor side in **175**. Located at the outer surface of the membrane, this charge repositioning inverted the orientation of the flipper along the lipid tails in the outer leaflet. This important change does not affect spectroscopic properties significantly. Elongation of the headgroup in **176-178** further decreases brightness and mechanosensitivity. Headgroup shortening by replacement of the turn-on sulfide with a 1,6 S-O chalcogen-bonding sulfonate **179** is better tolerated, although $I/I_0 = 0.52$ remains disappointing.

Within the spectroscopically convincing (Figure 18) but chemically fragile (Scheme 4) scaffold of **171**, oxidation of the donating sulfide bridge into the withdrawing sulfone bridge **180** produces two excitation maxima, one highly mechanosensitive, the other not, either an artefact or an interesting observation that deserves further investigation (compare dithienodiketophosphepin **125**, Figure 9).[90,152] The monomeric push-pull analog **181** without planarizable bond connecting two DTT flipper naturally lost all mechanosensitivity. Extension of the conjugated system with thiophenes in strong push-pull systems **182** and **183** shifts the excitation maxima to the red but reduces mechanosensitivity and brightness.[135]

The operational probes **157** and, in model membrane, also **171**, have been characterized extensively. Depth quenching supports alignment along lipid tails with little repositioning upon phase transition.[152] Partition coefficients reveal remarkably little preference among different phases. Langmuir-Blodgett (LB) isotherms of monolayers at the air-water interface suggest that the structure of surrounding phospholipid membranes is not affected (as it is, for instance, by the presence of cholesterol).[171] Compatibility with detection by second-harmonic generation (SHG) at biomimetic interfaces has been confirmed.[172]

To image forces in living cells, only Flipper-TR™ **157** is acceptable, **170** and **171** are too cytotoxic, possibly due to headgroup elimination (Scheme 4).[173] Fluorescence lifetime imaging microscopy (FLIM) was selected for detection because the response is concentration independent. To calibrate forces with FLIM response, GUVs were aspirated with micropipettes, and the produced forces were quantified from

the diameter of membrane nanotubes pulled from the GUV with optical tweezers (Figure 20C). For membranes that cannot separate into different domains, the fluorescence lifetime τ of flipper **157** decreases linearly with the tension σ applied to the membranes (Figure 20C). This response is as expected for lipid decompression and flipper deplanarization as response to increasing tension (Figure 20A). For membranes that can separate into different domains, the average τ increases linearly with σ until saturation is reached. This response is consistent with tension-induced assembly and disassembly of microdomains that sort out lipids that cannot be stretched (Figure 20B). With little preference in partitioning but oscillator strength increasing with planarization, the average response is then dominated by emission from planar probes in highly-ordered microdomains. Consistent with previous reports,[174,175] tension-induced self-sorting into microdomains could be directly observed in GUVs (Figure 20D).

In all cells tested, lifetimes of force probes **157** increase with increasing tension. This result suggests that the response of Flipper-TR™ **157** to increasing tension in cells is dominated by the assembly of highly ordered microdomains to sort out "unstretchable" lipids, whereas the response to decreasing tension is dominated by the disassembly of the same, highly ordered microdomains. Different slopes are found for force-lifetime curves with different cells. This is meaningful because the composition of their plasma membranes changes, and implies that force-lifetime calibration curves are always required for quantitative measurements. However, a quasi-linear increase of lifetimes with tension is observed for all cells tested. This suggests that tension-induced membrane reorganization, the assembly and the disassembly of unstretchable microdomains, is general. The functional relevance of tension-induced membrane reorganization is thus expected to be important and general, for example to regulate signal transduction cascades, as exemplified with force probe **157** for TORC2, the target of rapamycin complex 2.[176]
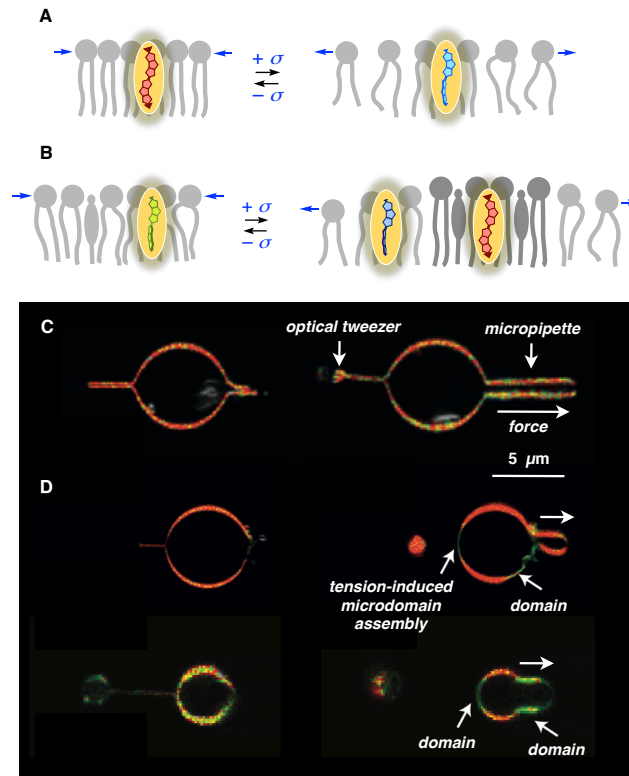
Figure 20. (A) Lipid decompression by membrane tension σ is reported by force probe **157** in membranes that cannot phase separate: Fluorescent lifetimes in FLIM images of GUVs decrease with increasing tension applied with micropipettes and measured with optical tweezers (C). (B) Tension-induced microdomain (dis)assembly of "unstretchable" lipids is reported in membranes that can phase separate (DOPC/SM/CL): More and less ordered domains appear, average fluorescence lifetimes increase with increasing tension (D). The color code represents fluorescence lifetimes from 5.5 ns (red) to 4.0 ns (blue). Adapted with permission from ref. 173. Copyright 2018 Springer-Nature.

Flipper-TR™ **157** selectively labels the plasma membrane (Figure 21). To label specific membrane domains, the formation of dynamic covalent boronate esters **195** with vicinal diols in the headgroup of gangliosides, particularly sialic acid, was considered first.[177] Against close controls such as **196**, boronic acids were introduced into the headgroup of flippers **197** and **198**. For more general targeting,

41

biotinylated flipper probes **199** were prepared. Interfacing with the tetravalent streptavidin should allow to selectively label any biotinylated target of free choice. The formation of complex **200** with biotinylated lipids was elaborated as example. Detailed methods development provided access to the selective labeling of biotinylated membranes in GUVs and cells with the operational force probe **199**.[178]

Whereas Flipper-TR™ **157** is the first chemistry tool that provides access to fluorescence imaging of forces at cell surfaces, it can be argued that the study of external forces is also possible with physics tools such as micropipettes, optical tweezers, cantilevers of atomic force microscopes, and so on. However, these physical tools are obviously incompatible with the study of forces operating within living cells. To direct flipper probes to different organelles, established motifs known from the respective trackers were attached (Figure 21).[179] Morpholine bases in **201** label endosomes and lysosomes because their protonation at the lower pH within these organelles produces cationic headgroups that hinder release by diffusion across the membrane. ER flippers **202** are equipped with a thiol reactive pentafluorophenyl group and a very long, hydrophilic spacer to, presumably, react with protein disulfide isomerases (PDI) in the membrane of the endoplasmic reticulum. Mito flippers **203** feature the classical hydrophobic phosphonium cation that is attracted by the anionic mitochondrial membrane with high, inside negative membrane potential.

All probes show perfect co-localization with the trackers of the respective organelles. Their lifetime in different organelles differ because the composition of their membranes differs. However, they all respond uniformly with decreasing lifetime to decreasing membrane tension applied by osmotic stress. They thus provide unprecedented access to the detection and study of physical forces within cells. As an example, an increase in membrane tension in mitochondrial constriction sites, presumably on the way toward fission, was clearly detectable as locally increasing lifetimes in FLIM images, from 3.0 to 3.5 ns (Figure 21). These results suggest that flipper probes are ready as chemical tools to study questions in biology that have been of central interest but beyond reach for a long time.
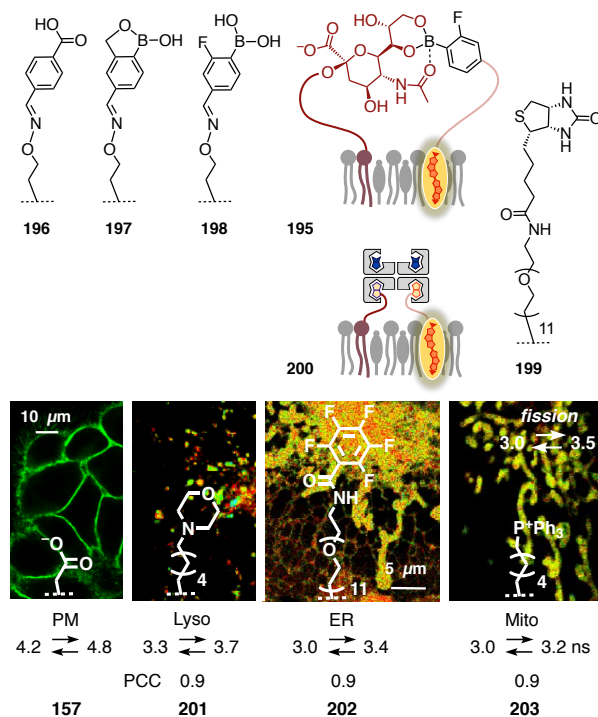
Figure 21. Fluorescent force probes that selectively target gangliosides (**195**, **197**, **198**), biotinylated lipids (**199**, **200**), the plasma membrane (PM, **157**), lysosomes (**201**), ER (**202**) and mitochondria (**203**), with selected CLSM (**157**) and FLIM images (**201–203**), lifetime changes in response to increasing membrane tension by osmotic stress (or mitochondrial constriction, in ns, and PCCs (Pearson's correlation coefficients) for co-localization with trackers; for R, see **157**, Figure 18). The FLIM color code represents fluorescence lifetimes from 4.5 ns (red) to 1.0 ns (blue). Adapted with permission from ref. 179. Copyright 2019 American Chemical Society.

10. PHOTOSYSTEMS

The appearance of DTTs in various photosystems will be covered in this chapter. The first subchapter focuses on push-pull systems and applications in non-linear optics and in functional materials such as dye-sensitized solar cells (DSSCs). The next subchapter summarizes DTTs in polymers and their use in functional materials such as light emitting diodes (LEDs), organic field-effect transistors (OFETs) and organic photovoltaics (OPVs). A special chapter is devoted to the self-assembly and templated assembly

of DTTs into thin films as well as fluorescent fibers, also along microtubules within living cells. The final subchapter bundles pioneering efforts toward the integration of DTTs into more complex photosystems.

10.1. PUSH-PULL SYSTEMS

DTTs, presenting a large π surface with efficient electron communication due to the mixing of the sulfur orbitals into the system, are attractive scaffolds for electron relay in push-pull, push-push or pull-pull systems in applications to non-linear optics (NLO) such as two-photon absorption (TPA) and second-harmonic generation (SHG), and in DSSCs. To create such properties, DTTs have been substituted with conjugated electronic donors (D) and acceptors (A). The synthesis and the properties of three D-DTT-A systems **204-206** have been reported in 2000 (Figure 22).[180] Only one of the push-pull systems is fluorescent. However, they all display an unusual reversed solvatochromic behavior. Increasing the polarity of the solvent leads to hypsochromic shifts, an effect that is more pronounced as the strength of the push-pull system increases. D-DTT-A systems are more stable and display higher hyperpolarizability than their polyene or thiophene equivalents, probably because of their extended π delocalization and the participation of the sulfur atoms in the delocalized system.[181] In the D-DTT-D and D-DTT-A systems **207-210**, D and A are linked to the DTT core by a vinyl linker.[182] Surprisingly no strong differences in TPA efficiency between the symmetric (**207**, **208**) and asymmetric (**209**, **210**) architectures are observed. They all display higher cross-section for TPA (σ_{TPA}) than reference compounds available at the time, such as **211**. The symmetric D-DTT-D **207** and **208** display an amphoteric electrochemical behavior, showing two reversible oxidation waves and one reduction wave. Interestingly, stable quinoid oxidized forms can aggregate into π dimers in both solution and solid phase.[183] Push-pull D-DTT-A **212** features an extended triphenylaryl core with two fluorenes as donors.[184] From this compound, the first DDT-based small-molecule DSSC reached a power conversion efficiency (PCE) of 7.0% with high photostability. The broad absorption and ease of synthesis of this triad encouraged the synthesis of several similar systems for solar energy conversion. D-DTT-A **213** has been synthesized by consecutive
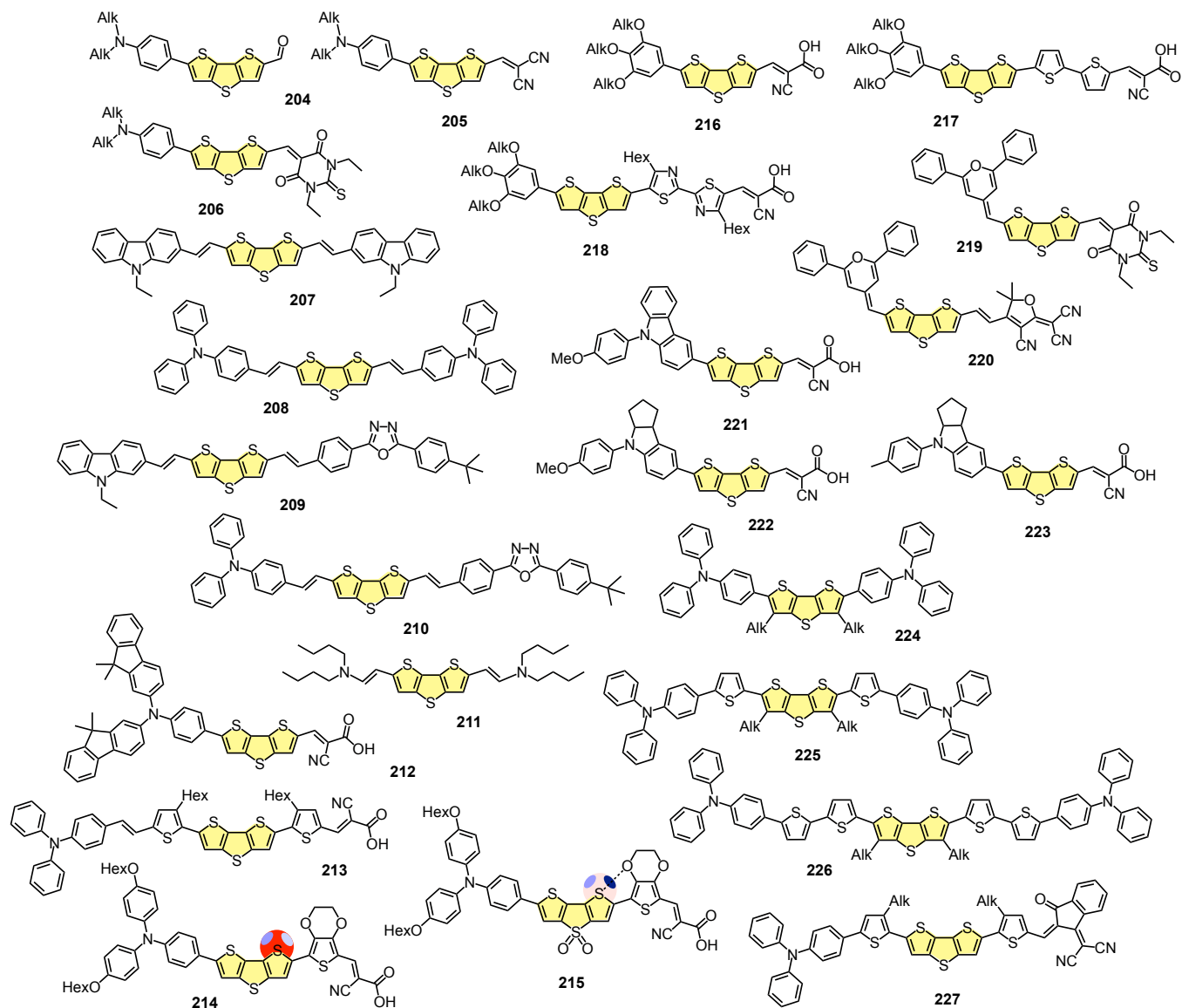
Figure 22. Push-pull and push-push DTT photosystems used in non-linear optics and dye-sensitized solar cells.

Wittig-Horner and Knoevenagel reactions on the symmetric bis-formylated dithiophene-DTT to provide a system covering a broad absorption in the solar spectrum with a high extinction coefficient.[185] Cyclic voltammetry reveals LUMO and HOMO levels that are compatible with those of the iodine/iodide couple and the TiO_2 conduction bands, which allowed the elaboration and test of a DSC displaying an power conversion efficiency of 7.3%. For similar applications, compounds **214** and **215** were synthesized from a succession of palladium-catalyzed cross-couplings yielding D-DTT-A systems with an electron-rich or

45

poor central unit.[186] These compounds display a broad absorption and a band gap compatible with DSSC technologies, and solar cells prepared from them show power conversion efficiencies of 2.7 and 6.1%, respectively. It should be noted that these compounds were compared to their equivalent featuring a 3-methylthieno[3,2-b]thiophene (MTT) unit, in reduced or oxidized (MTTO) forms instead of a DTT or DTTO2. While the MTT compound performs better than the DTT one (5.2 vs 4.2%), the opposite is observed comparing the MTTO to the DTTO2 bridged systems (2.7 vs 6.1%), possibly due to the better absorption properties. Aiming at improving the organization of DTT-based DSSC solar cells, compounds **216–218** presenting a tris(dodecyloxy)phenyl were synthesized. Π Extended compounds **217** and **218** present broad absorption compatible with DSSC applications. Push-pull DTT **217**, probably because it was the only one presenting mesomorphic properties, has been used to prepare the best performing DSSC compared to the two other prepared DTT-based dyes.[187] In 2013, NLO active push-pull DTTs **219** and **220** featuring pyranylidene donors were reported.[188] These compounds display broad absorption spectra with maxima located around 659 and 708 nm, respectively, probably due to a favorable intramolecular charge transfer (ICT). When it comes to electric field-induced second harmonic generation, they display good $\mu\beta_0$ values although they were outperformed by their thieno[3,2-b]thiophene (TT) equivalents. Carbazole and indoline-based D-DTT-A **221–223** were also synthesized for DSSC applications.[189] Indoline-based compounds reveal a more-red shifted and broader absorption compared to the carbazole equivalents. This was translated into better energy conversion efficiencies, highlighting indoline as an alternative donor in these D-DTT-A triads. Bis-triphenylamine D-DTT-D dyes **224–227** without or with thiophene and dithiophene spacers were synthesized for TPA applications.[190] These systems show strong emission in one-photon excitation with quantum yields between 43% and 67%. D-DTT-D **226** exhibits a high TPA cross section value but it is outperformed by tetrathienoacene (TTA) analogs also reported in this study, probably owing to their extended π-system. Recently, D-DTT-A **227** was reported as an electron donor for bulk-heterojunction solar cells using PC$_{71}$BM as an acceptor. However, **227** underperformed compared to the trithiophene homolog because of less-optimal electrochemical

46

properties.[191]   Overall, these push-pull and push-push systems support DTTs as a versatile and well-performing π linker, allowing for good communication between the donor and the acceptor and providing access to the synthesis of well-performing architectures in NLO and DSSC applications.
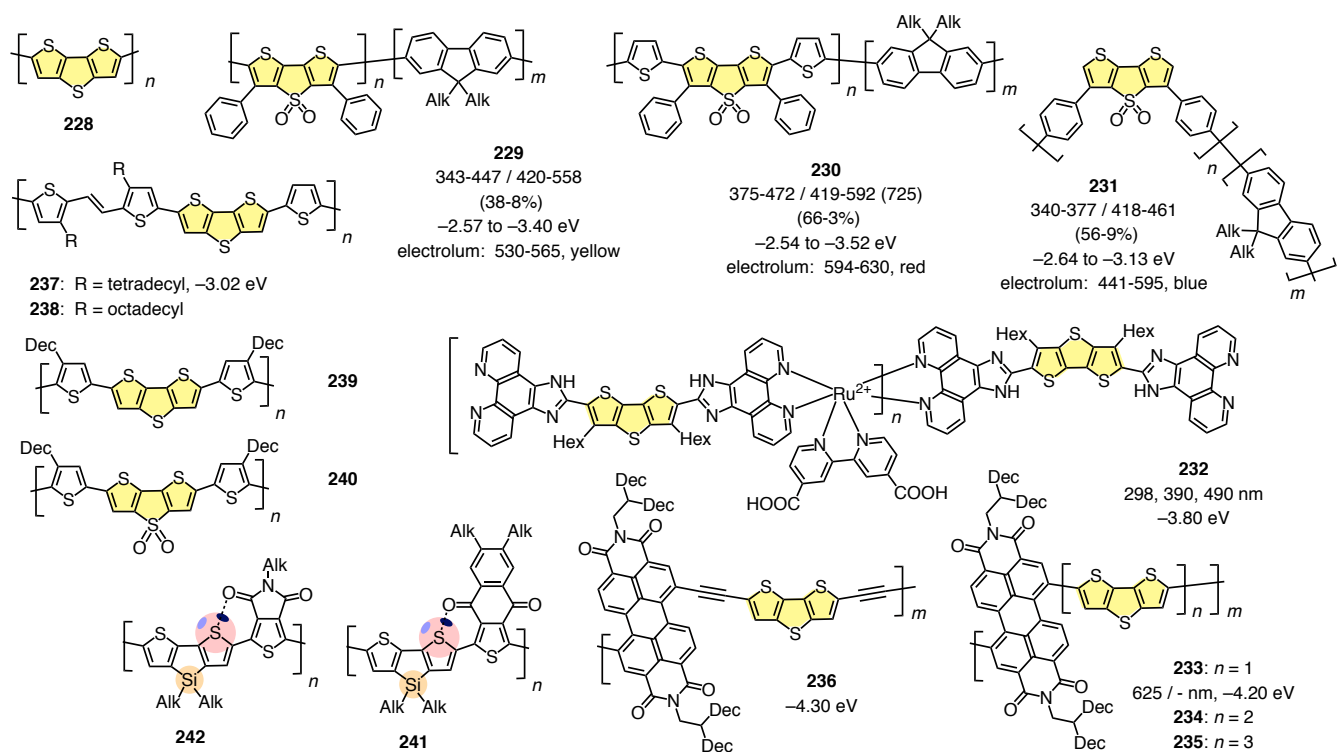
Figure 23. Polymeric photosystems with DTTs or close analogs (dithienosiloles), explored in the context of organic photovoltaics; with indication of pertinent absorption / emission maxima (in nm), quantum yields (in %), and LUMO energies (in eV vs –5.1 eV for Fc$^+$/Fc).

10.2. POLYMERS

The most productive and promising application of DTT-containing polymers as photoactive hole transporters in functional organic materials, particularly OPVs, has been reviewed extensively from different, more focused points of view.[12,15,16] The attention in this research is often directed more toward materials engineering than toward the chemical space of DTTs as emerging privileged scaffold. This subchapter will thus highlight only two specific aspects that are of high relevance for the topic of this

review. Polymers with DTT and particularly DTTO2 that contribute significantly to function will be covered first, followed by polymers with DTTs or analogs that explicitly consider contributions from σ hole interactions to function.

Pure poly(DTT)s **228** have been prepared by electropolymerization (Figure 23).[192] Five constitutional DTT isomers have been polymerized the same way. The n and p doping of the resulting conjugated polymers has been shown to depend strongly on the structure of the isomer. The use of the strong fluorescence of DTTO2 for LED applications has been explored with fluorene-DTTO2 copolymers **229–231**.[193] For all polymers, increasing length causes a red shift of absorption and emission and a decrease of fluorescence quantum yield and LUMO energy. Electroluminescence is mostly blue for the cross-conjugated **231**, yellow for the conjugated **229**, and red for **230** with extra thiophenes between fluorene and DTTO2.

DTTs have been integrated into metallopolymers such as **232**.[194] Their interesting electrochromism is, however, not dependent on the presence of the DTT. The carboxylic acids were installed for further interfacing with pyridyl-ZnO nanoparticles.

Co-polymers **233** composed of DTTs and perylenediimides (PDIs) have initiated the use of DTTs to organic photovoltaics (OPVs).[195] DTT-PDI copolymers **233** are solution processible, broadband absorbing and n transporting. Electron mobilities up to 1.3×10^{-2} cm^2 V^{-1} s^{-1} are among the highest known at that time for solution processed OFETs. Hole transport was not observed for donor-acceptor co-polymers **233**. HOMO levels at –3.90 eV are slightly below those of the most popular fullerene in OPVs (–4.20 eV, PCBM). Combined with a polythiophene as hole transporter, OPVs with average power conversion efficiencies larger that 1% were obtained. The insertion of one additional DTT in copolymers **234** increases LUMO levels to –4.10 eV and PCE to 1.08%, whereas the insertion of two additional DTTs in copolymers **235** decreases LUMO levels to –4.30 eV and PCE to 0.77%.[196,197] Acetylene spacers in co-polymers **236** lower the LUMO by 0.1 eV, shift the absorption by 89 nm to the red, and show increased

electron mobility in OFETs.[198] Donor-donor copolymers **237** and **238** provide access to hole mobilities in OFETs up to 3.91 cm^2 V^{-1} s^{-1}.[199] Absorption from 500 nm to 700 nm covers much of the visible range. Related copolymers **239** and **240** have been prepared early on as soluble poly(DTT)s and explored with regard to photoluminescence and photoinduced electron transfer to fullerenes and TiO$_2$.[200,201]

For OPV applications, co-polymers with DTTs and analogs have been tested with many different partners and many other atoms in the bridge.[71,89] Several of the monomers used have been covered in chapter 3.1. In the context of this review, interested in origins and uniqueness of the emerging multifunctionality of DTTs, the use of chalcogen bonding in OPV design deserves particular attention.[12,89,202–204]

A chalcogen bond from the dithienosilole to the 1,6 oxygen acceptor is expected to planarize the donor−acceptor copolymer **241**.[89,202] The resulting advantages in packing and charge mobility yield OPVs with PCEs up to 5.21%.[203,204] The same 1,6 S-O chalcogen bonds from dithienosilole (and germoles, cyclopentabithiophenes) to thieno[3,4-c]pyrrole-4,6-diones are computed to fully planarize copolymer **242**.[12,89,205,206] The results are high OFET charge mobilities and PCEs up to 6.83%. The compared to chalcogen-bond free controls high fill factors support the importance of chalcogen bonding for supramolecular organization.

10.3. SELF-ASSEMBLED SYSTEMS

10.3.1. OPTICAL DEVICES

The organizing power of intramolecular chalcogen bonding in DTTs and related 3,3'-fused dithiophenes has been expanded from polymers to self-assembling monomers. A comprehensive series from Bazan and coworkers focuses on DADAD motifs **243**–**250** (donor-acceptor-donor-acceptor-donor, Figure 24).[207–209] A central dithienosilole donor is combined with pyridathiadiazole acceptors and terminal donors. The extension of terminal thiophenes in **243** to bithiophenes in **245** is made to red shift absorption, that is to lower the bandgap. The power conversion efficiency of OPVs increases

correspondingly to 3.2%. In pentad **246**, intramolecular chalcogen bonds are installed to enforce co-planarity between the dithienosilole core and the flanking pyridathiadiazole acceptors. The results include OFETs with hole mobility of 0.2 cm^2 V^{-1} s^{-1} and OPVs from highly-organized co-assembly with fullerenes with 7.0% power conversion efficiency. Deletion of chalcogen bonds in control **248** yields poor charge mobility, poor PCE (0.2%) and poor self- and co-assembly. This focus on chalcogen bonds is driven to perfection in constitutional isomers **249** and **250**.[209] Their remarkably different optical thermal and self-assembly properties are shown to originate from chalcogen bonds that planarize but also bend isomers **249** (bend angle 112.0º) but not isomer **250** (116.1º) into a more banana-shaped global structure. Replacement of the silicon bridge in **249** by a germanium bridge increases bending (110.8º) as expected from strengthened chalcogen bonds, whereas carbon bridges cause the respective decrease in bending (bend angle 125.4º). Several other analogs of this series have been explored for high-efficiency OPVs.[210,211]
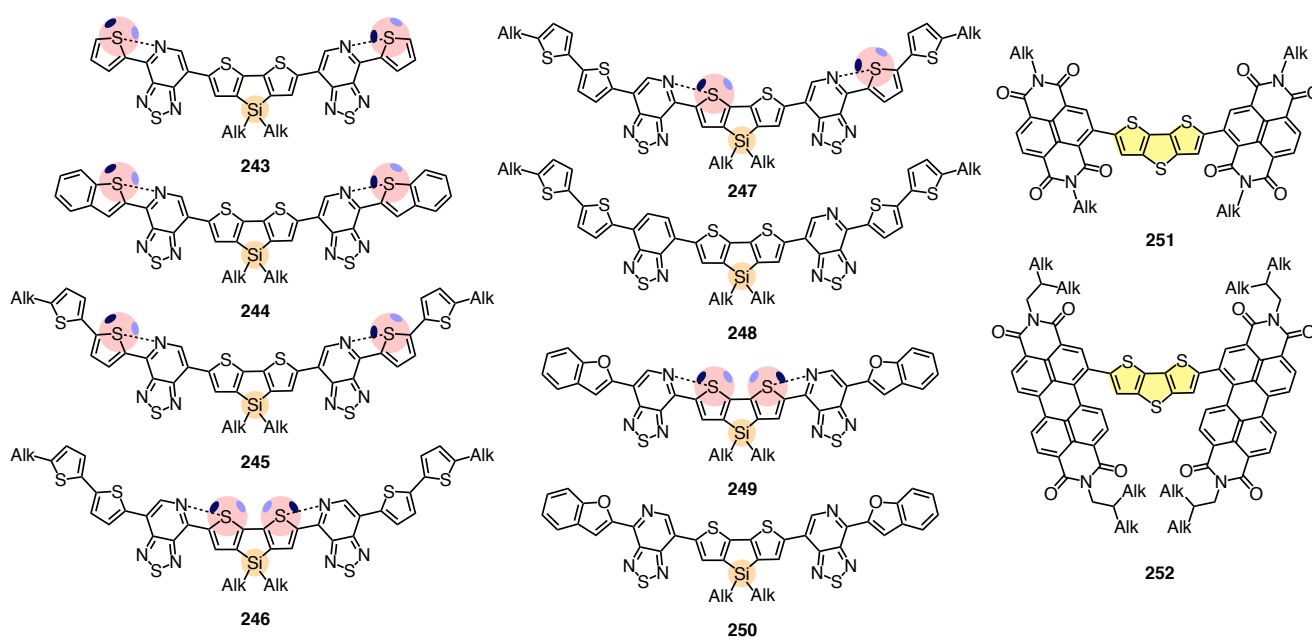
Figure 24. Self-assembling photosystems with DTT conjugates or close analogs.

The self-assembly of NDI-DTT-NDI triads **251** and PDI-DTT-PDI triads **252** has been explored for use in n-channel OFETs.[212,213] Comparison with other bridges did not reveal particular advantages with DTTs. 2,2'-DTT dimers **12** (Figure 3), equipped with terminal alkyl tails, have been shown to self-assemble into highly organized thin films.[214] With **20–22** (Figure 6), the sulfur redox switch has also been explored to improve self-assembly in highly ordered thin film and the resulting change mobilities.[23] The self-assembling packing of DTTs in single crystals has been extensively shown to be dominated by π-π interactions and chalcogen bonds (e.g., **16**, **26**, Figure 10A).

The self-assembly of DTTO2 attracted much attention because of the unusually strong fluorescence in the solid state. For DTTO2 **3**, it was shown early on that emission from the solid occurs at 513 nm with a quantum yield of 12%, compared to 446 nm and 75% in solution (Figure 3).[1] Similar with two methyls in **15**: Emission from the solid at 518 nm with a quantum yield of 16%. With peripheral phenyls in **18**, emission with 85% in solution drops to 24% in the solid. With the more deplanarizing peripheral thiophenes in **19**, the same record 85% in solution translates much better into 48% emission from the solid.

Since all DTTO2 show high electron affinities and ionization energies, they are promising candidates for (electro-)luminescent devices. An electroluminescent diode made from **18** shows low but still promising power conversion efficiency of 0.004%.[1] Exploitation of the DTT-structure in **253–255** yields bright white-light emitting diodes (Figure 25).[215] In solution, DTT **253** emits at 480 nm. Self-assembly into cross-like dimers in solid state affords a strongly red-shifted emission maximum at 680 nm. Fabrication of a device by spincoating DTT **253** between indium tin oxide (ITO) and poly(ethylenedioxythiophene):poly(styrenesulfonate) (PEDOT:PSS) or LiF and Al layers leads to white light electroluminescence. The white light is obtained by the superposition of the blue emission of the single molecule with the red-shifted emission of the crossed dimers. The electroluminescence spectrum shows similar features to the photoluminescence, although the low-energy peak is more intense.

Therefore, the obtained device exhibits a white-light electro-luminescence (EL) with a luminance of 3800 cd/m^2 at 18 V and an external quantum efficiency (QE) of 0.35%.

DTTs **254** and **255** were synthesized to investigate the effect of packing. DTT **254** shows poor brightness level, probably due to the lower number of boron atoms. DTTO2 **255** does not show any low-energy shifted additional peak in the EL spectrum. This is in agreement with the expected arrangement of the two perpendicularly arranged oxygen atoms, which prevents the formation of crossed dimers.[215]

With the elongated sexithiophene analogue **25**, OLETs could be obtained from films grown by vacuum sublimation and drop-casting (Figure 3).[216] They represent the first non-polymeric layer in a light emitting transistor made from solution-based techniques, here drop-casting.

10.3.2. INTRACELLULAR SELF-ASSEMBLY

In 2011, the Barbarella group discovered that compounds **18** and **256–258** spontaneously cross the membrane of living cells (Figure 25).[18,217,218] The compounds are poorly soluble in water, however all of them show the right hydrophilicity/hydrophobicity balance to cross the cellular membrane, after incubation for 1 h in buffered solutions. All four compounds stain the cytoplasm, but not the nucleus, and stain the cells for at least 7 days, without harm.

However, DTTO2 **18** and **256–258** uniformly stain the cytoplasm of cells only at the beginning. After 3-6 hours, they start to migrate to the perinuclear region, where they concentrate in multiple clusters, leading to fibril formation (until 12 hours). The fibrils show complex helical supramolecular structure, and it was demonstrated, that they are mainly made of type-I collagen. It was shown that this phenomenon is most probably due to the molecular recognition between compound **18** and the hydroxyproline component of the protocollagen polypeptide chains by hydrogen bonding. The resulting co-assembly in a triple helix is more stable than those that would be obtained by the self-assembly of the isolated building blocks. Nonetheless a staining of the cytoplasm can be observed even after fibril formation.
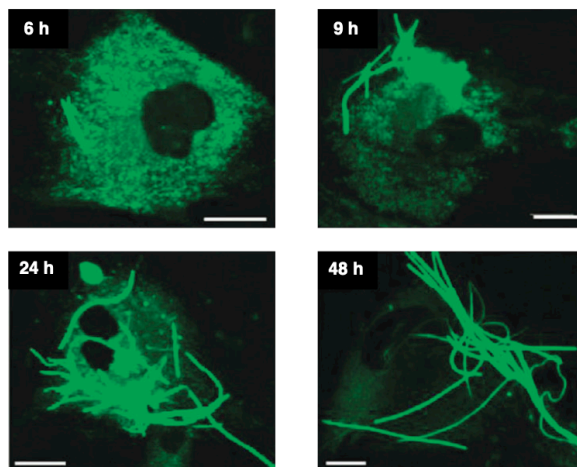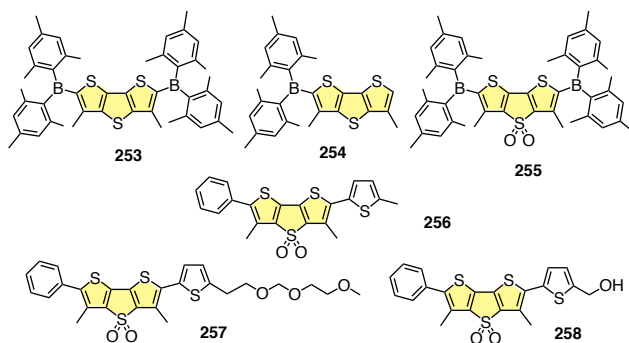
Figure 25. DTTs for self-assembly into white-fluorescent thin films and fluorescent fibers inside cells, with CLSM images of fluorescent fibers in bone-marrow human tumor fibroblasts incubated with 0.12 mM DTTO2 **18**. Scale bars: 10 μm. Adapted with permission from ref. 218. Copyright 2013 Oxford Academic.

The ability to form these fluorescent fibers is not limited to a certain kind of cells or proteins. It was demonstrated that the same phenomenon can be seen in HeLa cells, as well as mouse euroblastoma cells, in which microfibers with vimentin are formed.[219] These studies were recently extended to oligothiophenes.[220]

Star-shaped oligomers have emerged as attractive materials because, compared to their linear analogs, they show better solubility on the one hand and afford more ordered films on the other hand.[221] Star-shaped DTT tetramers **259** absorb at 460 nm and emit at 523 and 547 nm in solution (Figure 26). High LUMO energies at –3.05 eV are as expected and consistent with the transport of holes rather than electrons. In OFETs, hole mobilities of μ = 0.025 cm^2 V^{-1} s^{-1} were measured. This is orders of magnitudes faster than in the analogous thienothiophene and dithiophene star controls. This record activity with p-semiconducting DTT stars **259** was shown to originate from the spontaneous self-assembly into highly-ordered and oriented films, with smooth surface and without large crystallites. The high preorganization contributed by the DTTs to stars **259** in the ground state was confirmed by the comparably small Stokes shifts, implying that little conformational reorganization is necessary to reach planarization in relaxed excited states (compare chapter 9).

The [5]helicene-like fused DTT dimers **260** are accessible in 30% yield from the linear dimer **261**.[32] In crystal structures, the dihedral angle between the two central thiophenes is 5.6º. With selenium atoms substituted into the DTT core of analog **262**, this minimal helicity almost doubles to 10.6º. Both absorption and emission show strong vibrational bands, particularly at low temperature. Increasing selenium content causes small red shifts, lowers the LUMO slightly, and reduces fluorescence quantum yields significantly.

Diarylethenes are most popular because of their unique photochromism in crystals.[222] Photochromism is the photoinduced switching between two isomers with different absorption spectra. With diarylethenes, the photochromic transformation is the electrocyclization of formal 1,3,5-hexatrienes **263** into formal cyclohexadienes **264**. The integration of DTTs into diarylethenes is of interest to create p semiconductors with photoswitchable transport properties.[223–225] Best results were obtained with **263**: 71% yield for the photocyclization, red-shifted absorption of product **264** at 510 nm, and the lowest among the high LUMO energies at –3.71 eV.[223] Moving the aromatic extension from the diarylethene in **263** to the DTT side in

265 and twisting it a bit more reduces all these record values slightly. Moving the aromatic extension in between diarylethene and DTT at constant twist in **266** gives red-shifted cyclization products at lower yield of 53%. Removal of the aromatic extension in **267** restores the yield to 78% but blue shifts the absorption of the product up to almost 100 nm. Fused aromatic extensions in **268** give very poor cyclization yield.[224] In dimer **269**, only one diarylethene forms, the second photocyclization is inhibited by intramolecular energy transfer to the product chromophore. The DTT dimer **270** cyclizes in solution and LB monolayers but not in crystals, suggesting that asymmetric diarylethene are important for antiparallel packing in the crystal.[225]
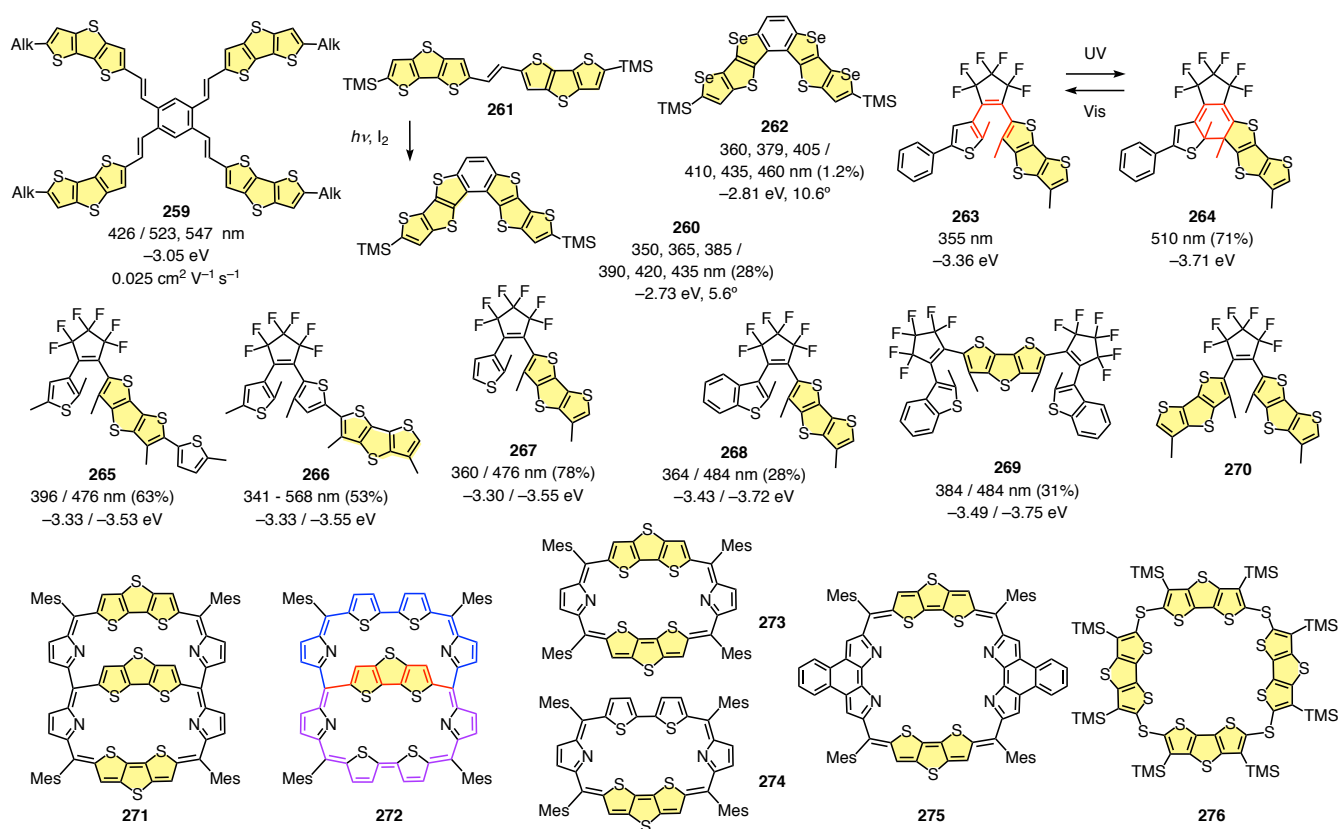
Figure 26. Integration of DTTs into more complex architectures, with indication of selected absorption / emission maxima in nm, in parenthesis fluorescence quantum or photoisomerization yields in %, LUMO energies (in eV vs −5.1 eV for Fc⁺/Fc), twist angle in degrees, biaromaticity (purple: shared; red, blue: not shared; **272**).

Bicylces **271** and **272** were designed to produce a 26π and a 34π aromatic circuit that are not coupled but share the same π electrons.[226] 26π Macrocycles are usually planar, as confirmed by models **273** and **274**. 34π Macrocycles, however, roll up into eight-shaped conformations. The DTT bridge in **271** and **272** is introduced to planarize the 34π circuit (blue) and overlay an equally conjugated 26π circuit (red) that shares some of the π electrons (purple, Figure 26). In the crystal structure, the presence of three DTTs forces the two macrocycles in **271** into near co-planarity, with the central DTT bridge twisted by 10º out of the plane of the 34π macrocycle. In **272**, removal of two out of three sulfide bridges in the DTTs increases the deviation of the remaining DTT bridge from the 34π macrocycle only slightly to 16º. These flattened bicycles provide sufficient orbital overlap in both aromatic circuits. Pertinent shifts in the NMR spectra confirm the existence of two separate ring currents, i.e., the biaromaticity of bicycles **271** and **272**. For instance, the β-CH protons of the DTT in bicycle **272** appear at 7.3 ppm in ¹H NMR spectrum. The downfield shift compared to the 10.7 ppm in macrocycle **273** demonstrates exposure to the ring current of the outside 34π circuit and, by resisting to shift below 7.3 ppm, also to the inside 26π circuit. In other words, the shift of the DTT β-CH protons in **272** evinces simultaneous exposure to shielding and deshielding ring currents, that is biaromaticity.

Absorption maxima of **272** at 501 and 605 nm are consistent with competing 26π and 34π aromatic systems (Figure 27). Two more maxima above 800 and 1000 nm are observed, emission occurs at 1100 nm. Upon oxidation, changes in the absorption spectra show that the 34π circuit reacts before the 26π circuit (Figure 27, left side). Complete oxidation produces a 33π and a 25π circuit, that is two overlayed [4n+1] systems. The total count of 40π electrons gives a [4n] system that is incompatible with the Hückel [4n+2] rule. However, the spectroscopic signature of the [4n] dication is that of an aromatic system. Such a reversal of the Hückel rule from [4n+2] to [4n] aromaticity in ground-state triplet biradicals is known in theory as Baird's rule but has never been observed before.

A related conjugated macrocycle **275** composed of two naphthobipyrroles and two DTTs has been reported separately in the context of proton-coupled redox switching (Figure 26).[227] With a 32π circuit,

macrocycle **275** is non-aromatic and absorbs below 600 nm. Full oxidation affords an aromatic 34π dication that absorbs up to 1200 nm.

Thiacalix[4]dithienophene **276**, composed of **4** DTTs linked by sulfur, could be isolated as main product in 43% from the random oligomerization of dibromo DTT in the presence of first BuLi and then Ph_2S_2 (Figure 26).[228] These macrocycles formed complexes with two C_{60}. The highly symmetrical structure of this complex yielded condensed strings of fullerenes in the co-crystal.
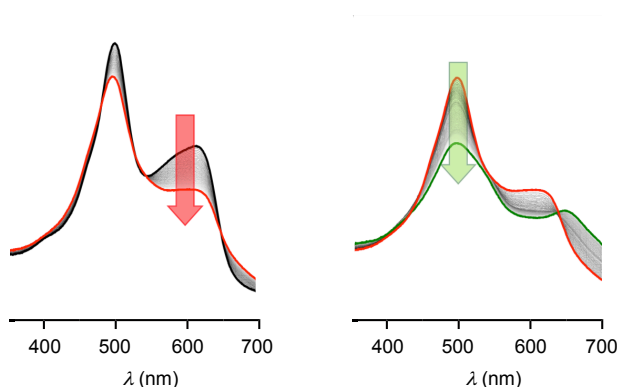
Figure 27. Absorption spectra of **272** during oxidative titrations at the first (0.65 V, left) and the second oxidation potential (1.10 V, right). Adapted with permission from ref. 226. Copyright 2017 Springer-Nature.

11. CONCLUSIONS

The objective of this review was to summarize the multifunctionality of dithieno[3,2-*b*:2',3'-*d*]thiophenes comprehensively, and to embed the result in a broader context.

DTTs – an emerging privileged scaffold, a future classic? Among the different functions covered, the fluorescent probes to image physical forces in biology are unique for DTTs and address a central challenge that is otherwise beyond reach. Other activities such as binding, transport and catalysis do so far not perform beyond the ordinary. In various photosystems, from organic solar cells to photochromes and anti-Hückel biaromatics, the presence of DTTs often does not appear really essential.

The origin of the unfolding multifunctionality of DTTs is quite promising for future growth. Intermolecular chalcogen bonds are just being recognized as high-precision tools in non-covalent functional architectures, and the DTT scaffold offers inward-outward chalcogen-bonding cascades of the simplicity and purity that distinguishes privileged scaffolds. The power of this motif is exemplified by the fact that the introduction of chalcogen bonds not only to transmembrane ion transport but also to catalysis has been realized with DTTs.

An unusual, versatile and inspiring combination of this chalcogen-bonding chemistry with i) sulfur redox switches in the bridge and ii) turn-on fluorescence ultimately accounts for most of the multifunctionality of the DTT scaffold. Efficient electron communication due to integrated sulfur orbitals, yielding maximal hyperpolarizability and charge mobilities, or a large, rigid and planarizing π surface, contributing to high-precision self-assembly into smooth films and fibrils, can be added to these key characteristics. An understanding of the structural space around the DTT scaffold, from heteroatom permutations to bridge expansion, is essential to assess the uniqueness of these characteristics. This knowledge is also needed to appreciate and possibly integrate related highlights such as the spectacular white fluorescence of twisted diketophosphepins or high-precision self-assembly into functional materials, including conformational control with chalcogen bonds in organic solar cells. While DTTs are synthetically accessible since almost five decades, it is important to note that most studies toward their multifunctionality are very recent. The lessons learned remain underexplored in more conventional functional systems for this reason. Their integration can thus be expected to provide access to functions that are otherwise beyond reach, as exemplified by the imaging of physical forces in biology or transport and catalysis with chalcogen bonds. We hope that this review will encourage new adventures in this direction.

AUTHOR INFORMATION

Corresponding Author

stefan.matile@unige.ch

Notes

Biographical Information

Karolina Strakova received her BS and her MS from University of Chemistry and Technology in Prague (2016) before starting her PhD in the Matile group.

Lea Assies received her BS and her MS from Humboldt University Berlin (2018) before starting her PhD in the Matile group.

Antoine Goujon received his PhD from Professor Nicolas Giuseppone at the University of Strasbourg (2016) before starting his postdoc in the Matile group.

Francesca Piazzolla received her PhD from Professor Andrea Temperini at the University of Perugia (2019) before starting her postdoc in the Matile group.

Heorhii V. Humeniuk received his BS from University of Kyiv (2017) and his MS as a Werner fellow from the Matile group before starting his PhD in the same group.

Stefan Matile is a professor at the University of Geneva; PhD: University of Zurich, Switzerland; postdoc: Columbia University, USA.

ACKNOWLEDGMENTS

REFERENCES

(1) Barbarella, G.; Favaretto, L.; Sotgiu, G.; Antolini, L.; Gigli, G.; Cingolani, R.; Bongini, A. Rigid-Core Oligothiophene-*S,S*-Dioxides with High Photoluminescence Efficiencies Both in Solution and in

the Solid State. *Chem. Mater.* **2001**, *13*, 4112–4122.

(2) Zhao, Y.; Cotelle, Y.; Liu, L.; López-Andarias, J.; Bornhof, A.-B.; Akamatsu, M.; Sakai, N.; Matile, S. The Emergence of Anion−π Catalysis. *Acc. Chem. Res.* **2018**, *51*, 2255–2263.

(3) Dado, G. P.; Gellman, S. H. Redox Control of Secondary Structure in a Designed Peptide. *J. Am. Chem. Soc.* **1993**, *115*, 12609–12610.

(4) Sakai, N.; Gerard, D.; Matile, S. Electrostatics of Cell Membrane Recognition: Structure and Activity of Neutral and Cationic Rigid Push-Pull Rods in Isoelectric, Anionic, and Polarized Lipid Bilayer Membranes. *J. Am. Chem. Soc.* **2001**, *123*, 2517–2524.

(5) Míšek, J.; Vargas Jentzsch, A.; Sakurai, S.; Emery, D.; Mareda, J.; Matile, S. A Chiral and Colorful Redox Switch: Enhanced π Acidity in Action. *Angew. Chem. Int. Ed.* **2010**, *49*, 7680–7683.

(6) Kawabata, K.; Takeguchi, M.; Goto, H. Optical Activity of Heteroaromatic Conjugated Polymer Films Prepared by Asymmetric Electrochemical Polymerization in Cholesteric Liquid Crystals: Structural Function for Chiral Induction. *Macromolecules* **2013**, *46*, 2078–2091.

(7) Kurimoto, Y.; Mitsudo, K.; Mandai, H.; Wakamiya, A.; Murata, Y.; Mori, H.; Nishihara, Y.; Suga, S. Efficient Synthesis and Properties of Benzothieno[3,2-*b*]thieno[2,3-*d*]furans and Benzothieno[3,2-*b*]thieno[2,3-*d*]thiophenes. *Asian J. Org. Chem.* **2018**, *7*, 1635–1641.

(8) Benz, S.; Macchione, M.; Verolet, Q.; Mareda, J.; Sakai, N.; Matile, S. Anion Transport with Chalcogen Bonds. *J. Am. Chem. Soc.* **2016**, *138*, 9093–9096.

(9) Ozturk, T.; Ertas, E.; Mert, O. Dithienothiophenes. *Tetrahedron* **2005**, *61*, 11055–11077.

(10) Cinar, M. E.; Ozturk, T. Thienothiophenes, Dithienothiophenes, and Thienoacenes: Syntheses, Oligomers, Polymers, and Properties. *Chem. Rev.* **2015**, *115*, 3036–3140.

(11) Mishra, A.; Ma, C.-Q.; Bäuerle, P. Functional Oligothiophenes: Molecular Design for Multidimensional Nanoarchitectures and Their Applications. *Chem. Rev.* **2009**, *109*, 1141–1276.

(12) Huang, H.; Yang, L.; Facchetti, A.; Marks, T. J. Organic and Polymeric Semiconductors Enhanced by Noncovalent Conformational Locks. *Chem. Rev.* **2017**, *117*, 10291–10318.

(13)   Romero-Nieto, C.; Baumgartner, T. Dithieno[3,2-*b*:2′,3′-*d*]phospholes: A Look Back at the First Decade. *Synlett* **2013**, *24*, 920–937.

(14)   Baumgartner, T. Insights on the Design and Electron-Acceptor Properties of Conjugated Organophosphorus Materials. *Acc. Chem. Res.* **2014**, *47*, 1613–1622.

(15)   Coppo, P.; Turner, M. L. Cyclopentadithiophene Based Electroactive Materials. *J. Mater. Chem.* **2005**, *15*, 1123-1133.

(16)   Ohshita, J. Group 14 Metalloles Condensed with Heteroaromatic Systems. *Org. Photonics Photovolt.* **2016**, *4*, 54-59.

(17)   Roncali, J.; Blanchard, P.; Frère, P. 3,4-Ethylenedioxythiophene (EDOT) as a Versatile Building Block for Advanced Functional π-Conjugated Systems. *J. Mater. Chem.* **2005**, *15*, 1589–1610.

(18)   Barbarella, G.; Di Maria, F. Supramolecular Oligothiophene Microfibers Spontaneously Assembled on Surfaces or Coassembled with Proteins inside Live Cells. *Acc. Chem. Res.* **2015**, *48*, 2230–2241.

(19)   Li, X.-C.; Sirringhaus, H.; Garnier, F.; Holmes, A. B.; Moratti, S. C.; Feeder, N.; Clegg, W.; Teat, S. J.; Friend, R. H. A Highly π-Stacked Organic Semiconductor for Thin Film Transistors Based on Fused Thiophenes. *J. Am. Chem. Soc.* **1998**, *120*, 2206–2207.

(20)   San Miguel, L.; Porter, W. W.; Matzger, A. J. Planar β-Linked Oligothiophenes Based on Thieno[3,2-*b*]thiophene and Dithieno[3,2-*b*:2‘,3‘-*d*]thiophene Fused Units. *Org. Lett.* **2007**, *9*, 1005–1008.

(21)   He, M.; Zhang, F. Synthesis and Structure of Alkyl-Substituted Fused Thiophenes Containing up to Seven Rings. *J. Org. Chem.* **2007**, *72*, 442–451.

(22)   Janssen, M. J.; De Jong, F. Synthesis, Oxidation, and Electronic Spectra of Four Dithienothiophenes. *J. Org. Chem.* **1971**, *36*, 1645–1648.

(23)   Santato, C.; Favaretto, L.; Melucci, M.; Zanelli, A.; Gazzano, M.; Monari, M.; Isik, D.; Banville, D.; Bertolazzi, S.; Loranger, S.; Cicoira F. Influence of the Oxidation Level on the Electronic,

Morphological and Charge Transport Properties of Novel Dithienothiophene S-Oxide and S,S-Dioxide Inner Core Oligomers. *J. Mater. Chem.* **2010**, *20*, 669–676.

(24)   Hong, W.; Yuan, H.; Li, H.; Yang, X.; Gao, X.; Zhu, D. Linear Fused Dithieno[2,3-*b*:3′2′-*d*]thiophene Diimides. *Org. Lett.* **2011**, *13*, 1410–1413.

(25)   Benz, S.; López-Andarias, J.; Mareda, J.; Sakai, N.; Matile, S. Catalysis with Chalcogen Bonds. *Angew. Chem. Int. Ed.* **2017**, *56*, 812–815.

(26)   Hansch, C.; Leo, A.; Taft, R. W. A Survey of Hammett Substituent Constants and Resonance and Field Parameters. *Chem. Rev.* **1991**, *91*, 165–195.

(27)   Shefer, N.; Harel, T.; Rozen, S. Synthesis of Oxygenated Fused Oligothiophenes with HOF·CH$_3$CN. *J. Org. Chem.* **2009**, *74*, 6993–6998.

(28)   De Jong, F.; Janssen, M. J. Synthesis of Dithienothiophenes. *J. Org. Chem.* **1971**, *36*, 1998–2000.

(29)   Sakai, N.; Mareda, J.; Vauthey, E.; Matile, S. Core-Substituted Naphthalenediimides. *Chem. Commun.* **2010**, *46*, 4225–4237.

(30)   Kondo, R.; Yasuda, T.; Yang, Y. S.; Kim, J. Y.; Adachi, C. Highly Luminescent π-Conjugated Dithienometalloles: Photophysical Properties and Their Application in Organic Light-Emitting Diodes. *J. Mater. Chem.* **2012**, *22*, 16810–16816.

(31)   Kozmík, V.; Pozník, M.; Svoboda, J.; Frére, P. Dithieno[3,2-*b*:2′,3′-*d*]furan as a New Building Block for Fused Conjugated Systems. *Tetrahedron Lett.* **2015**, *56*, 6251–6253.

(32)   Xu, W.; Wang, M.; Ma, Z.; Shan, Z.; Li, C.; Wang, H. Selenophene-Based Heteroacenes: Synthesis, Structures, and Physicochemical Behaviors. *J. Org. Chem.* **2018**, *83*, 12154–12163.

(33)   Barlow, S.; Odom, S. A.; Lancaster, K.; Getmanenko, Y. A.; Mason, R.; Coropceanu, V.; Brédas, J.-L.; Marder, S. R. Electronic and Optical Properties of 4 *H*-Cyclopenta[2,1-*b*:3,4-*b′*]bithiophene Derivatives and Their 4-Heteroatom-Substituted Analogues: A Joint Theoretical and Experimental Comparison. *J. Phys. Chem. B* **2010**, *114*, 14397–14407.

(34)   Polander, L. E.; Pandey, L.; Barlow, S.; Tiwari, S. P.; Risko, C.; Kippelen, B.; Brédas, J.-L.; Marder, S. R. Benzothiadiazole-Dithienopyrrole Donor–Acceptor–Donor and Acceptor–Donor–Acceptor Triads: Synthesis and Optical, Electrochemical, and Charge-Transport Properties. *J. Phys. Chem. C* **2011**, *115*, 23149–23163.

(35)   Lu, H.-I.; Lu, C.-W.; Lee, Y.-C.; Lin, H.-W.; Lin, L.-Y.; Lin, F.; Chang, J.-H.; Wu, C.-I.; Wong, K.-T. New Molecular Donors with Dithienopyrrole as the Electron-Donating Group for Efficient Small-Molecule Organic Solar Cells. *Chem. Mater.* **2014**, *26*, 4361–4367.

(36)   Yue, W.; Zhao, Y.; Shao, S.; Tian, H.; Xie, Z.; Geng, Y.; Wang, F. Novel NIR-Absorbing Conjugated Polymers for Efficient Polymer Solar Cells: Effect of Alkyl Chain Length on Device Performance. *J. Mater. Chem.* **2009**, *19*, 2199–2206.

(37)   Zhou, E.; Wei, Q.; Yamakawa, S.; Zhang, Y.; Tajima, K.; Yang, C.; Hashimoto, K. Diketopyrrolopyrrole-Based Semiconducting Polymer for Photovoltaic Device with Photocurrent Response Wavelengths up to 1.1 μm. *Macromolecules* **2010**, *43*, 821–826.

(38)   Yue, W.; Huang, X.; Yuan, J.; Ma, W.; Krebs, F. C.; Yu, D. A Novel Benzodipyrrolidone-Based Low Band Gap Polymer for Organic Solar Cells. *J. Mater. Chem. A* **2013**, *1*, 10116–10119.

(39)   Zhang, X.; Shim, J. W.; Tiwari, S. P.; Zhang, Q.; Norton, J. E.; Wu, P.-T.; Barlow, S.; Jenekhe, S. A.; Kippelen, B.; Brédas, J.-L.; Marder S. R. Dithienopyrrole–Quinoxaline/Pyridopyrazine Donor–Acceptor Polymers: Synthesis and Electrochemical, Optical, Charge-Transport, and Photovoltaic Properties. *J. Mater. Chem.* **2011**, *21*, 4971–4982.

(40)   Grisorio, R.; Allegretta, G.; Suranna, G. P.; Mastrorilli, P.; Loiudice, A.; Rizzo, A.; Mazzeo, M.; Gigli, G. Monodispersed vs. Polydispersed Systems for Bulk Heterojunction Solar Cells: The Case of Dithienopyrrole/Anthracene Based Materials. *J. Mater. Chem.* **2012**, *22*, 19752–19760.

(41)   Liu, J.; Zhang, R.; Sauvé, G.; Kowalewski, T.; McCullough, R. D. Highly Disordered Polymer Field Effect Transistors: *N*-Alkyl Dithieno[3,2-*b* :2′,3′-*d*]pyrrole-Based Copolymers with Surprisingly High Charge Carrier Mobilities. *J. Am. Chem. Soc.* **2008**, *130*, 13167–13176.

(42)   Baumgartner, T.; Neumann, T.; Wirges, B. The Dithieno[3,2-*b*:2′,3′-*d*]phosphole System: A Novel Building Block for Highly Luminescent π-Conjugated Materials. *Angew. Chem. Int. Ed.* **2004**, *43*, 6197–6201.

(43)   Ren, Y.; Kan, W. H.; Henderson, M. A.; Bomben, P. G.; Berlinguette, C. P.; Thangadurai, V.; Baumgartner, T. External-Stimuli Responsive Photophysics and Liquid Crystal Properties of Self-Assembled "Phosphole-Lipids." *J. Am. Chem. Soc.* **2011**, *133*, 17014–17026.

(44)   Ren, Y.; Dienes, Y.; Hettel, S.; Parvez, M.; Hoge, B.; Baumgartner, T. Highly Fluorinated Dithieno[3,2-*b* :2′,3′-*d*]phospholes with Stabilized LUMO Levels. *Organometallics* **2009**, *28*, 734–740.

(45)   Gaffen, J. R.; Bentley, J. N.; Torres, L. C.; Chu, C.; Baumgartner, T.; Caputo, C. B. A Simple and Effective Method of Determining Lewis Acidity by Using Fluorescence. *Chem* **2019**, *5*, 1567-1583.

(46)   Kato, T.; Imoto, H.; Tanaka, S.; Ishidoshiro, M.; Naka, K. Facile Synthesis and Properties of Dithieno[3,2-*b*:2′,3′-*d*]arsoles. *Dalton Trans.* **2016**, *45*, 11338–11345.

(47)   Imoto, H.; Kawashima, I.; Yamazawa, C.; Tanaka, S.; Naka, K. Multi-Mode Emission Color Tuning of Dithieno[3,2-*b*:2′,3′-*d*]arsoles. *J. Mater. Chem. C* **2017**, *5*, 6697–6703.

(48)   Green, J. P.; Gupta, A. K.; Orthaber, A. Effect of Arsenic Coordination State on the Structure, Aromaticity, and Optical Properties of Dithieno[3,2-*b*:2′,3′-*d*]arsoles. *Eur. J. Inorg. Chem.* **2019**, *2019*, 1539–1543.

(49)   Ohshita, J.; Fujita, R.; Tanaka, D.; Ooyama, Y.; Kobayashi, N.; Higashimura, H.; Yamamoto, Y. Synthesis and Optical Properties of Dithienostiboles. *Chem. Lett.* **2012**, *41*, 1002–1003.

(50)   Ohshita, J.; Matsui, S.; Yamamoto, R.; Mizumo, T.; Ooyama, Y.; Harima, Y.; Murafuji, T.; Tao, K.; Kuramochi, Y.; Kaikoh, T.; Higashimura H. Synthesis of Dithienobismoles as Novel Phosphorescence Materials. *Organometallics* **2010**, *29*, 3239–3241.

(51)   Willot, P.; Cremer, L. D.; Koeckelberghs, G. The Use of Cyclopenta[2,1-*b*;3,4-*b′*]dithiophene Analogues for the Development of Low-Bandgap Materials. *Macromol. Chem. Phys.*

2012, *213*, 1216–1224.

(52)   Azoulay, J. D.; Koretz, Z. A.; Wong, B. M.; Bazan, G. C. Bridgehead Imine Substituted Cyclopentadithiophene Derivatives: An Effective Strategy for Band Gap Control in Donor–Acceptor Polymers. *Macromolecules* **2013**, *46*, 1337–1342.

(53)   Wang, Z.; Putta, A.; Mottishaw, J. D.; Wei, Q.; Wang, H.; Sun, H. Molecular Origin of Isomerization Effects on Solid State Structures and Optoelectronic Properties: A Comparative Case Study of Isomerically Pure Dicyanomethylene Substituted Fused Dithiophenes. *J. Phys. Chem. C* **2013**, *117*, 16759–16768.

(54)   Lee, K.-H.; Ohshita, J.; Tanaka, D.; Tominaga, Y.; Kunai, A. Synthesis and Optical Properties of Spirobi(dithienometallole)s and Spirobi(dithienothiametalline)s. *J. Organomet. Chem.* **2012**, *710*, 53–58.

(55)   Ohshita, J.; Nakamura, M.; Ooyama, Y. Preparation and Reactions of Dichlorodithienogermoles. *Organometallics* **2015**, *34*, 5609–5614.

(56)   Tanaka, D.; Ohshita, J.; Ooyama, Y.; Kobayashi, N.; Higashimura, H.; Nakanishi, T.; Hasegawa, Y. Synthesis, Optical Properties, and Crystal Structures of Dithienostannoles. *Organometallics* **2013**, *32*, 4136–4141.

(57)   Kim, D.-H.; Ohshita, J.; Lee, K.-H.; Kunugi, Y.; Kunai, A. Synthesis of π-Conjugated Oligomers Containing Dithienosilole Units. *Organometallics* **2006**, *25*, 1511–1516.

(58)   Ohshita, J.; Lee, K.-H.; Hashimoto, M.; Kunugi, Y.; Harima, Y.; Yamashita, K.; Kunai, A. Preparation of 4,4-Diaryl-2-(tricyanoethenyl)dithienosiloles and Vapor-Chromic Behavior of the Film. *Org. Lett.* **2002**, *4*, 1891–1894.

(59)   Ohshita, J.; Tanaka, D.; Lee, K.-H.; Kurushima, Y.; Kajiwara, S.; Ooyama, Y.; Harima, Y.; Kunai, A.; Kunugi, Y. Synthesis and Chromic Behaviors of Dithienosiloles with Push-Pull Substituents Toward VOC Detection. *Mol. Cryst. Liq. Cryst.* **2010**, *529*, 1–9.

(60)   Adachi, Y.; Nomura, T.; Ohshita, J. Intramolecular Energy Transfer in Dithienogermole

Derivatives. *Chem. Eur. J.* **2019**, *25*, 4974–4983.

(61)   Ohshita, J.; Lee, K.-H.; Hamamoto, D.; Kunugi, Y.; Ikadai, J.; Kwak, Y.-W.; Kunai, A. Synthesis of Novel Spiro-Condensed Dithienosiloles and the Application to Organic FET. *Chem. Lett.* **2004**, *33*, 892–893.

(62)   Braunschweig, H.; Fernández, I.; Frenking, G.; Kupfer, T. Structural Evidence for Antiaromaticity in Free Boroles. *Angew. Chem. Int. Ed.* **2008**, *47*, 1951–1954.

(63)   Iida, A.; Yamaguchi, S. Thiophene-Fused Ladder Boroles with High Antiaromaticity. *J. Am. Chem. Soc.* **2011**, *133*, 6952–6955.

(64)   Cao, H.; Brettell-Adams, I. A.; Qu, F.; Rupar, P. A. Bridged Difurans: Stabilizing Furan with p-Block Elements. *Organometallics* **2017**, *36*, 2565–2572.

(65)   Getmanenko, Y. A.; Purcell, T. A.; Hwang, D. K.; Kippelen, B.; Marder, S. R. Easily Reducible Materials from the Reactions of Diselenopheno[3,2-*b*:2′,3′-*d*]pyrrole and Dithieno[3,2-*b*:2′,3′-*d*]pyrrole with Tetracyanoethylene. *J. Org. Chem.* **2012**, *77*, 10931–10937.

(66)   Pao, Y.-C.; Chen, Y.-L.; Chen, Y.-T.; Cheng, S.-W.; Lai, Y.-Y.; Huang, W.-C.; Cheng, Y.-J. Synthesis and Molecular Properties of Tricyclic Biselenophene-Based Derivatives with Nitrogen, Silicon, Germanium, Vinylidene, and Ethylene Bridges. *Org. Lett.* **2014**, *16*, 5724–5727.

(67)   Farnier, M.; Soth, S.; Fournari, P. Recherches en série hétérocyclique. XXVIII. Synthèse de bipyrroles. *Can. J. Chem.* **1976**, *54*, 1083–1086.

(68)   Arad, O.; Morros, J.; Batllori, X.; Teixidó, J.; Nonell, S.; Borrell, J. I. Diethyl 2,7-Dibromo-4H,5H-thieno[3,2-*b*:4,5-*b*']dipyrrole-3,6-Dicarboxylate: A Key Intermediate for a Diversity Oriented Synthesis of 2,7,12,17-Tetraarylporphycenes. *Org. Lett.* **2006**, *8*, 847–850.

(69)   Shefer, N.; Rozen, S. Synthesis of Oxidized Thienopyrroles Using HOF·CH₃CN. *J. Org. Chem.* **2011**, *76*, 4611–4616.

(70)   Krutosikova, A.; Dandarova, M. Substitued Vinyl Azides in Synthesis of Furo[3,2-*b*:4,5-*b*']diplyrroles and Pyrrolo[2',3':4,5]furo[3,2-*c*]pyridines. *Heterocycles* **1994**, *37*, 1695–1700.

(71)   Patra, D.; Lee, J.; Dey, S.; Lee, J.; Kalin, A. J.; Putta, A.; Fei, Z.; McCarthy-Ward, T.; Bazzi, H. S.; Fang, L.; Heeney, M.; Yoon, M.-H.; Al-Hashimi M. Chalcogen Bridged Thieno- and Selenopheno[2,3-*d*:5,4-*d'*]bisthiazole and Their Diketopyrrolopyrrole Based Low-Bandgap Copolymers. *Macromolecules* **2018**, *51*, 6076–6084.

(72)   Getmanenko, Y. A.; Singh, S.; Sandhu, B.; Wang, C.-Y.; Timofeeva, T.; Kippelen, B.; Marder, S. R. Pyrrole[3,2-*d*:4,5-*d'*]bisthiazole-Bridged Bis(Naphthalene Diimide)s as Electron-Transport Materials. *J. Mater. Chem. C* **2014**, *2*, 124–131.

(73)   Uzelac, E. J.; McCausland, C. B.; Rasmussen, S. C. Pyrrolo[2,3-*d* :5,4-*d'*]bisthiazoles: Alternate Synthetic Routes and a Comparative Study to Analogous Fused-Ring Bithiophenes. *J. Org. Chem.* **2018**, *83*, 664–671.

(74)   Al-Hashimi, M.; Labram, J. G.; Watkins, S.; Motevalli, M.; Anthopoulos, T. D.; Heeney, M. Synthesis and Characterization of Fused Pyrrolo[3,2-*d* :4,5-*d'*]bisthiazole-Containing Polymers. *Org. Lett.* **2010**, *12*, 5478–5481.

(75)   Patra, D.; Lee, J.; Lee, J.; Sredojevic, D. N.; White, A. J. P.; Bazzi, H. S.; Brothers, E. N.; Heeney, M.; Fang, L.; Yoon, M.-H.; Al-Hashimi M. Synthesis of Low Band Gap Polymers Based on Pyrrolo[3,2-*d*:4,5-*d'*]bisthiazole (PBTz) and Thienylenevinylene (TV) for Organic Thin-Film Transistors (OTFTs). *J. Mater. Chem. C* **2017**, *5*, 2247–2258.

(76)   He, X.; Woo, A. Y. Y.; Borau-Garcia, J.; Baumgartner, T. Dithiazolo[5,4-*b*:4',5'-*d*]phosphole: A Highly Luminescent Electron-Accepting Building Block. *Chem. Eur. J.* **2013**, *19*, 7620–7630.

(77)   Green, J. P.; Cryer, S. J.; Marafie, J.; White, A. J. P.; Heeney, M. Synthesis of a Luminescent Arsolo[2,3-*d*:5,4-*d'*]bis(thiazole) Building Block and Comparison to Its Phosphole Analogue. *Organometallics* **2017**, *36*, 2632–2636.

(78)   Getmanenko, Y. A.; Risko, C.; Tongwa, P.; Kim, E.-G.; Li, H.; Sandhu, B.; Timofeeva, T.; Brédas, J.-L.; Marder, S. R. Mono- and Dicarbonyl-Bridged Tricyclic Heterocyclic Acceptors:

Synthesis and Electronic Properties. *J. Org. Chem.* **2011**, *76*, 2660–2671.

(79)   Yuan, M.; Rice, A. H.; Luscombe, C. K. Benzo[2,1-*b*;3,4-*b*']dithiophene-Based Low-Bandgap Polymers for Photovoltaic Applications. *J. Polym. Sci. Part Polym. Chem.* **2011**, *49*, 701–711.

(80)   Xiao, S.; Zhou, H.; You, W. Conjugated Polymers of Fused Bithiophenes with Enhanced π-Electron Delocalization for Photovoltaic Applications. *Macromolecules* **2008**, *41*, 5688–5696.

(81)   Zhou, H.; Yang, L.; Stoneking, S.; You, W. A Weak Donor−Strong Acceptor Strategy to Design Ideal Polymers for Organic Solar Cells. *ACS Appl. Mater. Interfaces* **2010**, *2*, 1377–1383.

(82)   Morisaki, Y.; Tominaga, M.; Chujo, Y. Synthesis and Properties of Thiophene-Fused Benzocarborane. *Chem. Eur. J.* **2012**, *18*, 11251–11257.

(83)   Hayashi, N.; Saito, Y.; Zhou, X.; Yoshino, J.; Higuchi, H.; Mutai, T. A Comparative Study of the Electronic Spectra, Fluorescence Quantum Yields, Cyclic Voltammograms and Theoretical Calculations of Phenanthrene-Type Benzodifurans. *Tetrahedron* **2016**, *72*, 4159–4168.

(84)   Chen, W.; Tan, S. Y.; Zhao, Y.; Zhang, Q. A Concise Method to Prepare Novel Fused Heteroaromatic Diones through Double Friedel–Crafts Acylation. *Org. Chem. Front.* **2014**, *1*, 391–394.

(85)   Čibová, A.; Martinická, A.; Magdolen, P.; Zahradník, P.; Cigáň, M.; Uherek, M.; Chorvát, D. Dicationic and Monocationic Benzobisthiazolium Salts as Potential NLO Chromophores. *Dyes Pigments* **2018**, *149*, 597–611.

(86)   Benz, S.; Mareda, J.; Besnard, C.; Sakai, N.; Matile, S. Catalysis with Chalcogen Bonds: Neutral Benzodiselenazole Scaffolds with High-Precision Selenium Donors of Variable Strength. *Chem. Sci.* **2017**, *8*, 8164–8169.

(87)   Benz, S.; Besnard, C.; Matile, S. Chalcogen-Bonding Catalysis: From Neutral to Cationic Benzodiselenazole Scaffolds. *Helv. Chim. Acta* **2018**, *101*, e1800075.

(88)   Letizia, J. A.; Salata, M. R.; Tribout, C. M.; Facchetti, A.; Ratner, M. A.; Marks, T. J. N-Channel Polymers by Design: Optimizing the Interplay of Solubilizing Substituents, Crystal Packing, and Field-Effect Transistor Characteristics in Polymeric Bithiophene-Imide Semiconductors. *J. Am. Chem.*

Soc. **2008**, *130*, 9679–9694.

(89) Guo, X.; Zhou, N.; Lou, S. J.; Hennek, J. W.; Ponce Ortiz, R.; Butler, M. R.; Boudreault, P.-L. T.; Strzalka, J.; Morin, P.-O.; Leclerc, M.; Navarette J. T.; Ratner M. A.; Chen L. X.; Chang R. P. H.; Facchetti A.; Marks T. J. Bithiopheneimide–Dithienosilole/Dithienogermole Copolymers for Efficient Solar Cells: Information from Structure–Property–Device Performance Correlations and Comparison to Thieno[3,4-*c*]pyrrole-4,6-dione Analogues. *J. Am. Chem. Soc.* **2012**, *134*, 18427–18439.

(90) He, X.; Borau-Garcia, J.; Woo, A. Y. Y.; Trudel, S.; Baumgartner, T. Dithieno[3,2-*c*:2′,3′-*e*]-2,7-diketophosphepin: A Unique Building Block for Multifunctional π-Conjugated Materials. *J. Am. Chem. Soc.* **2013**, *135*, 1137–1147.

(91) Humeniuk, H. V.; Rosspeintner, A.; Licari, G.; Kilin, V.; Bonacina, L.; Vauthey, E.; Sakai, N.; Matile, S. White-Fluorescent Dual-Emission Mechanosensitive Membrane Probes That Function by Bending Rather than Twisting. *Angew. Chem. Int. Ed.* **2018**, *57*, 10559–10563.

(92) Zhou, Z.; Chen, D.-G.; Saha, M. L.; Wang, H.; Li, X.; Chou, P.-T.; Stang, P. J. Designed Conformation and Fluorescence Properties of Self-Assembled Phenazine-Cored Platinum(II) Metallacycles. *J. Am. Chem. Soc.* **2019**, *141*, 5535–5543.

(93) Zhang, Z.; Wu, Y.-S.; Tang, K.-C.; Chen, C.-L.; Ho, J.-W.; Su, J.; Tian, H.; Chou, P.-T. Excited-State Conformational/Electronic Responses of Saddle-Shaped *N,N′*-Disubstituted-Dihydrodibenzo[*a,c*]phenazines: Wide-Tuning Emission from Red to Deep Blue and White Light Combination. *J. Am. Chem. Soc.* **2015**, *137*, 8509–8520.

(94) He, X.; Baumgartner, T. Synthesis and Properties of a Dicationic π-Extended Dithieno[3,2-*c* :2′,3′-*e*]-2,7-diketophosphepin. *Organometallics* **2013**, *32*, 7625–7628.

(95) Macchione, M.; Chuard, N.; Sakai, N.; Matile, S. Planarizable Push–Pull Probes: Overtwisted Flipper Mechanophores. *ChemPlusChem* **2017**, *82*, 1062–1066.

(96) Hellberg, J.; Remonen, T. Tetramethyldithienothiophenes; New Donors for Cation Radical Salts. *Synth. Met.* **1995**, *70*, 1137–1138.

(97)   Frey, J.; Bond, A. D.; Holmes, A. B. Improved Synthesis of Dithieno[3,2-*b*:2′,3′-*d*]thiophene (DTT) and Derivatives for Cross Coupling. *Chem. Commun.* **2002**, 2424–2425.

(98)   Bauzá, A.; Mooibroek, T. J.; Frontera, A. The Bright Future of Unconventional σ/π-Hole Interactions. *ChemPhysChem* **2015**, *16*, 2496–2517.

(99)   Lim, J. Y. C.; Beer, P. D. Sigma-Hole Interactions in Anion Recognition. *Chem* **2018**, *4*, 731–783.

(100)   Beno, B. R.; Yeung, K.-S.; Bartberger, M. D.; Pennington, L. D.; Meanwell, N. A. A Survey of the Role of Noncovalent Sulfur Interactions in Drug Design. *J. Med. Chem.* **2015**, *58*, 4383–4438.

(101)   Gleiter, R.; Haberhauer, G.; Werz, D. B.; Rominger, F.; Bleiholder, C. From Noncovalent Chalcogen–Chalcogen Interactions to Supramolecular Aggregates: Experiments and Calculations. *Chem. Rev.* **2018**, *118*, 2010–2041.

(102)   Mahmudov, K. T.; Kopylovich, M. N.; Guedes da Silva, M. F. C.; Pombeiro, A. J. L. Chalcogen Bonding in Synthesis, Catalysis and Design of Materials. *Dalton Trans.* **2017**, *46*, 10121–10138.

(103)   Vogel, L.; Wonner, P.; Huber, S. M. Chalcogen Bonding: An Overview. *Angew. Chem. Int. Ed.* **2019**, *58*, 1880–1891.

(104)   Ho, H.-A.; Najari, A.; Leclerc, M. Optical Detection of DNA and Proteins with Cationic Polythiophenes. *Acc. Chem. Res.* **2008**, *41*, 168–178.

(105)   Biot, N.; Bonifazi, D. Programming Recognition Arrays through Double Chalcogen-Bonding Interactions. *Chem. Eur. J.* **2018**, *24*, 5439–5443.

(106)   Cavallo, G.; Metrangolo, P.; Milani, R.; Pilati, T.; Priimagi, A.; Resnati, G.; Terraneo, G. The Halogen Bond. *Chem. Rev.* **2016**, *116*, 2478–2601.

(107)   Borissov, A.; Marques, I.; Lim, J. Y. C.; Félix, V.; Smith, M. D.; Beer, P. D. Anion Recognition in Water by Charge-Neutral Halogen and Chalcogen Bonding Foldamer Receptors. *J. Am.*

Chem. Soc. **2019**, *141*, 4119–4129.

(108)   Warzok, U.; Marianski, M.; Hoffmann, W.; Turunen, L.; Rissanen, K.; Pagel, K.; Schalley, C. A. Surprising Solvent-Induced Structural Rearrangements in Large [N···I⁺···N] Halogen-Bonded Supramolecular Capsules: An Ion Mobility-Mass Spectrometry Study. *Chem. Sci.* **2018**, *9*, 8343–8351.

(109)   Riwar, L.-J.; Trapp, N.; Root, K.; Zenobi, R.; Diederich, F. Supramolecular Capsules: Strong versus Weak Chalcogen Bonding. *Angew. Chem. Int. Ed.* **2018**, *57*, 17259–17264.

(110)   Ams, M. R.; Trapp, N.; Schwab, A.; Milić, J. V.; Diederich, F. Chalcogen Bonding "2S–2N Squares" versus Competing Interactions: Exploring the Recognition Properties of Sulfur. *Chem. Eur. J.* **2019**, *25*, 323–333.

(111)   Sarwar, M. G.; Ajami, D.; Theodorakopoulos, G.; Petsalakis, I. D.; Rebek, J. Amplified Halogen Bonding in a Small Space. *J. Am. Chem. Soc.* **2013**, *135*, 13672–13675.

(112)   Takezawa, H.; Murase, T.; Resnati, G.; Metrangolo, P.; Fujita, M. Halogen-Bond-Assisted Guest Inclusion in a Synthetic Cavity. *Angew. Chem. Int. Ed.* **2015**, *54*, 8411–8414.

(113)   Pascoe, D. J.; Ling, K. B.; Cockroft, S. L. The Origin of Chalcogen-Bonding Interactions. *J. Am. Chem. Soc.* **2017**, *139*, 15160–15167.

(114)   Robertson, C. C.; Wright, J. S.; Carrington, E. J.; Perutz, R. N.; Hunter, C. A.; Brammer, L. Hydrogen Bonding vs. Halogen Bonding: The Solvent Decides. *Chem. Sci.* **2017**, *8*, 5392–5398.

(115)   Ho, P. C.; Rafique, J.; Lee, J.; Lee, L. M.; Jenkins, H. A.; Britten, J. F.; Braga, A. L.; Vargas-Baca, I. Synthesis and Structural Characterisation of the Aggregates of Benzo-1,2-chalcogenazole 2-Oxides. *Dalton Trans.* **2017**, *46*, 6570–6579.

(116)   Chen, L.; Xiang, J.; Zhao, Y.; Yan, Q. Reversible Self-Assembly of Supramolecular Vesicles and Nanofibers Driven by Chalcogen-Bonding Interactions. *J. Am. Chem. Soc.* **2018**, *140*, 7079–7082.

(117)   Scilabra, P.; Terraneo, G.; Resnati, G. The Chalcogen Bond in Crystalline Solids: A World

Parallel to Halogen Bond. *Acc. Chem. Res.* **2019**, *52*, 1313–1324.

(118)   Fabbro, C.; Armani, S.; Carloni, L.-E.; Leo, F. D.; Wouters, J.; Bonifazi, D. 2,5-Diamide-Substituted Five-Membered Heterocycles: Challenging Molecular Synthons. *Eur. J. Org. Chem.* **2014**, *2014*, 5487–5500.

(119)   Lim, J. Y. C.; Marques, I.; Thompson, A. L.; Christensen, K. E.; Félix, V.; Beer, P. D. Chalcogen Bonding Macrocycles and [2]Rotaxanes for Anion Recognition. *J. Am. Chem. Soc.* **2017**, *139*, 3122–3133.

(120)   Garrett, G. E.; Gibson, G. L.; Straus, R. N.; Seferos, D. S.; Taylor, M. S. Chalcogen Bonding in Solution: Interactions of Benzotelluradiazoles with Anionic and Uncharged Lewis Bases. *J. Am. Chem. Soc.* **2015**, *137*, 4126–4133.

(121)   Zhao, H.; Gabbaï, F. P. A Bidentate Lewis Acid with a Telluronium Ion as an Anion-Binding Site. *Nat. Chem.* **2010**, *2*, 984–990.

(122)   Scheiner, S. Highly Selective Halide Receptors Based on Chalcogen, Pnicogen, and Tetrel Bonds. *Chem. Eur. J.* **2016**, *22*, 18850–18858.

(123)   Sánchez-Sanz, G.; Trujillo, C. Improvement of Anion Transport Systems by Modulation of Chalcogen Interactions: The Influence of Solvent. *J. Phys. Chem. A* **2018**, *122*, 1369–1377.

(124)   Benz, S.; Poblador-Bahamonde, A. I.; Low-Ders, N.; Matile, S. Catalysis with Pnictogen, Chalcogen, and Halogen Bonds. *Angew. Chem. Int. Ed.* **2018**, *57*, 5408–5412.

(125)   Wonner, P.; Vogel, L.; Düser, M.; Gomes, L.; Kniep, F.; Mallick, B.; Werz, D. B.; Huber, S. M. Carbon–Halogen Bond Activation by Selenium-Based Chalcogen Bonding. *Angew. Chem. Int. Ed.* **2017**, *56*, 12009–12012.

(126)   Wonner, P.; Vogel, L.; Kniep, F.; Huber, S. M. Catalytic Carbon–Chlorine Bond Activation by Selenium-Based Chalcogen Bond Donors. *Chem. Eur. J.* **2017**, *23*, 16972–16975.

(127)   Yang, M.; Tofan, D.; Chen, C.-H.; Jack, K. M.; Gabbaï, F. P. Digging the Sigma-Hole of Organoantimony Lewis Acids by Oxidation. *Angew. Chem. Int. Ed.* **2018**, *57*, 13868–13872.

(128)   Arokianathar, J. N.; Frost, A. B.; Slawin, A. M. Z.; Stead, D.; Smith, A. D. Isothiourea-Catalyzed Enantioselective Addition of 4-Nitrophenyl Esters to Iminium Ions. *ACS Catal.* **2018**, *8*, 1153–1160.

(129)   Birman, V. B.; Li, X. Homobenzotetramisole: An Effective Catalyst for Kinetic Resolution of Aryl-Cycloalkanols. *Org. Lett.* **2008**, *10*, 1115–1118.

(130)   Gale, P. A.; Davis, J. T.; Quesada, R. Anion Transport and Supramolecular Medicinal Chemistry. *Chem. Soc. Rev.* **2017**, *46*, 2497–2519.

(131)   Lisbjerg, M.; Valkenier, H.; Jessen, B. M.; Al-Kerdi, H.; Davis, A. P.; Pittelkow, M. Biotin[6]uril Esters: Chloride-Selective Transmembrane Anion Carriers Employing C—H···Anion Interactions. *J. Am. Chem. Soc.* **2015**, *137*, 4948–4951.

(132)   Chuard, N.; Fujisawa, K.; Morelli, P.; Saarbach, J.; Winssinger, N.; Metrangolo, P.; Resnati, G.; Sakai, N.; Matile, S. Activation of Cell-Penetrating Peptides with Ionpair−π Interactions and Fluorophiles. *J. Am. Chem. Soc.* **2016**, *138*, 11264–11271.

(133)   Gorteau, V.; Bollot, G.; Mareda, J.; Perez-Velasco, A.; Matile, S. Rigid Oligonaphthalenediimide Rods as Transmembrane Anion−π Slides. *J. Am. Chem. Soc.* **2006**, *128*, 14788–14789.

(134)   Vargas Jentzsch, A.; Matile, S. Transmembrane Halogen-Bonding Cascades. *J. Am. Chem. Soc.* **2013**, *135*, 5302–5303.

(135)   Macchione, M.; Tsemperouli, M.; Goujon, A.; Mallia, A. R.; Sakai, N.; Sugihara, K.; Matile, S. Mechanosensitive Oligodithienothiophenes: Transmembrane Anion Transport Along Chalcogen-Bonding Cascades. *Helv. Chim. Acta* **2018**, *101*, e1800014.

(136)   Lee, L. M.; Tsemperouli, M.; Poblador-Bahamonde, A. I.; Benz, S.; Sakai, N.; Sugihara, K.; Matile, S. Anion Transport with Pnictogen Bonds in Direct Comparison with Chalcogen and Halogen Bonds. *J. Am. Chem. Soc.* **2019**, *141*, 810–814.

(137)   Sotgiu, G.; Zambianchi, M.; Barbarella, G.; Aruffo, F.; Cipriani, F.; Ventola, A. Rigid-

Core Fluorescent Oligothiophene-*S*,*S*-Dioxide Isothiocyanates. Synthesis, Optical Characterization, and Conjugation to Monoclonal Antibodies. *J. Org. Chem.* **2003**, *68*, 1512–1520.

(138)   Sotgiu, G.; Barbarella, G. Synthesis of Photostable Amine-Reactive Fluorescent Dyes by Postsynthetic Conversion of Bromide Dithienothiophene Derivatives. *J. Org. Chem.* **2007**, *72*, 4925–4931.

(139)   Leiphart, R. J.; Chen, D.; Peredo, A. P.; Loneker, A. E.; Janmey, P. A. Mechanosensing at Cellular Interfaces. *Langmuir* **2018**, *35*, 7509–7519.

(140)   Krieg, M.; Fläschner, G.; Alsteens, D.; Gaub, B. M.; Roos, W. H.; Wuite, G. J. L.; Gaub, H. E.; Gerber, C.; Dufrêne, Y. F.; Müller, D. J. Atomic Force Microscopy-Based Mechanobiology. *Nat. Rev. Phys.* **2019**, *1*, 41–57.

(141)   Diz-Muñoz, A.; Weiner, O. D.; Fletcher, D. A. In Pursuit of the Mechanics That Shape Cell Surfaces. *Nat. Phys.* **2018**, *14*, 648–652.

(142)   Roca-Cusachs, P.; Conte, V.; Trepat, X. Quantifying Forces in Cell Biology. *Nat. Cell Biol.* **2017**, *19*, 742–751.

(143)   Pontes, B.; Monzo, P.; Gauthier, N. C. Membrane Tension: A Challenging but Universal Physical Parameter in Cell Biology. *Semin. Cell Dev. Biol.* **2017**, *71*, 30–41.

(144)   Fin, A.; Vargas Jentzsch, A.; Sakai, N.; Matile, S. Oligothiophene Amphiphiles as Planarizable and Polarizable Fluorescent Membrane Probes. *Angew. Chem. Int. Ed.* **2012**, *51*, 12736–12739.

(145)   Baumeister, B.; Matile, S. Rigid-Rod β-Barrels as Lipocalin Models: Probing Confined Space by Carotenoid Encapsulation. *Chem. Eur. J.* **2000**, *6*, 1739–1749.

(146)   Gamiz-Hernandez, A. P.; Angelova, I. N.; Send, R.; Sundholm, D.; Kaila, V. R. I. Protein-Induced Color Shift of Carotenoids in β-Crustacyanin. *Angew. Chem. Int. Ed.* **2015**, *54*, 11564–11566.

(147)   Begum, S.; Cianci, M.; Durbeej, B.; Falklöf, O.; Hädener, A.; Helliwell, J. R.; Helliwell, M.; Regan, A. C.; Watt, C. I. F. On the Origin and Variation of Colors in Lobster Carapace. *Phys. Chem.*

Chem. Phys. **2015**, *17*, 16723–16732.

(148)   Kiser, P. D.; Golczak, M.; Palczewski, K. Chemistry of the Retinoid (Visual) Cycle. *Chem. Rev.* **2014**, *114*, 194–232.

(149)   Sheves, M.; Nakanishi, K.; Honig, B. Through-Space Electrostatic Effects in Electronic Spectra. Experimental Evidence for the External Point-Charge Model of Visual Pigments. *J. Am. Chem. Soc.* **1979**, *101*, 7086–7088.

(150)   Doval, D. A.; Molin, M. D.; Ward, S.; Fin, A.; Sakai, N.; Matile, S. Planarizable Push–Pull Oligothiophenes: In Search of the Perfect Twist. *Chem. Sci.* **2014**, *5*, 2819–2825.

(151)   Dal Molin, M.; Matile, S. 3,4-Ethylenedioxythiophene in Planarizable Push–Pull Oligothiophenes. *Org. Biomol. Chem.* **2013**, *11*, 1952.

(152)   Dal Molin, M.; Verolet, Q.; Colom, A.; Letrun, R.; Derivery, E.; Gonzalez-Gaitan, M.; Vauthey, E.; Roux, A.; Sakai, N.; Matile, S. Fluorescent Flippers for Mechanosensitive Membrane Probes. *J. Am. Chem. Soc.* **2015**, *137*, 568–571.

(153)   Soleimanpour, S.; Colom, A.; Derivery, E.; Gonzalez-Gaitan, M.; Roux, A.; Sakai, N.; Matile, S. Headgroup Engineering in Mechanosensitive Membrane Probes. *Chem. Commun.* **2016**, *52*, 14450–14453.

(154)   Klymchenko, A. S. Solvatochromic and Fluorogenic Dyes as Environment-Sensitive Probes: Design and Biological Applications. *Acc. Chem. Res.* **2017**, *50*, 366–375.

(155)   Xiong, Y.; Vargas Jentzsch, A.; Osterrieth, J. W. M.; Sezgin, E.; Sazanovich, I. V.; Reglinski, K.; Galiani, S.; Parker, A. W.; Eggeling, C.; Anderson, H. L. Spironaphthoxazine Switchable Dyes for Biological Imaging. *Chem. Sci.* **2018**, *9*, 3029–3040.

(156)   Kulkarni, R. U.; Miller, E. W. Voltage Imaging: Pitfalls and Potential. *Biochemistry* **2017**, *56*, 5171–5177.

(157)   Haidekker, M. A.; Theodorakis, E. A. Ratiometric Mechanosensitive Fluorescent Dyes: Design and Applications. *J. Mater. Chem. C* **2016**, *4*, 2707–2718.

(158)   Chambers, J. E.; Kubánková, M.; Huber, R. G.; López-Duarte, I.; Avezov, E.; Bond, P. J.; Marciniak, S. J.; Kuimova, M. K. An Optical Technique for Mapping Microviscosity Dynamics in Cellular Organelles. *ACS Nano* **2018**, *12*, 4398–4407.

(159)   Yang, Z.; He, Y.; Lee, J.-H.; Park, N.; Suh, M.; Chae, W.-S.; Cao, J.; Peng, X.; Jung, H.; Kang, C.; Kim J. S. A Self-Calibrating Bipartite Viscosity Sensor for Mitochondria. *J. Am. Chem. Soc.* **2013**, *135*, 9181–9185.

(160)   Sherin, P. S.; López-Duarte, I.; Dent, M. R.; Kubánková, M.; Vyšniauskas, A.; Bull, J. A.; Reshetnikova, E. S.; Klymchenko, A. S.; Tsentalovich, Y. P.; Kuimova, M. K. Visualising the Membrane Viscosity of Porcine Eye Lens Cells Using Molecular Rotors. *Chem. Sci.* **2017**, *8*, 3523–3528.

(161)   Vyšniauskas, A.; Balaz, M.; Anderson, H. L.; Kuimova, M. K. Dual Mode Quantitative Imaging of Microscopic Viscosity Using a Conjugated Porphyrin Dimer. *Phys. Chem. Chem. Phys.* **2015**, *17*, 7548–7554.

(162)   Klymchenko, A. S.; Demchenko, A. P. Electrochromic Modulation of Excited-State Intramolecular Proton Transfer: The New Principle in Design of Fluorescence Sensors. *J. Am. Chem. Soc.* **2002**, *124*, 12372–12379.

(163)   Baumgart, T.; Hunt, G.; Farkas, E. R.; Webb, W. W.; Feigenson, G. W. Fluorescence Probe Partitioning between L_o/L_d Phases in Lipid Membranes. *Biochim. Biophys. Acta* **2007**, *1768*, 2182–2194.

(164)   Liu, F.; Wu, T.; Cao, J.; Cui, S.; Yang, Z.; Qiang, X.; Sun, S.; Song, F.; Fan, J.; Wang, J.; Peng X. Ratiometric Detection of Viscosity Using a Two-Photon Fluorescent Sensor. *Chem. Eur. J.* **2013**, *19*, 1548–1553.

(165)   Guo, R.; Yin, J.; Ma, Y.; Wang, Q.; Lin, W. A Novel Mitochondria-Targeted Rhodamine Analogue for the Detection of Viscosity Changes in Living Cells, Zebra Fish and Living Mice. *J. Mater. Chem. B* **2018**, *6*, 2894–2900.

(166)   Li, L.-L.; Li, K.; Li, M.-Y.; Shi, L.; Liu, Y.-H.; Zhang, H.; Pan, S.-L.; Wang, N.; Zhou,

Q.; Yu, X.-Q. BODIPY-Based Two-Photon Fluorescent Probe for Real-Time Monitoring of Lysosomal Viscosity with Fluorescence Lifetime Imaging Microscopy. *Anal. Chem.* **2018**, *90*, 5873–5878.

(167)   López-Duarte, I.; Chairatana, P.; Wu, Y.; Pérez-Moreno, J.; Bennett, P. M.; Reeve, J. E.; Boczarow, I.; Kaluza, W.; Hosny, N. A.; Stranks, S. D.; Nicholas, R. J., Clays, K.; Kuimova, M. K.; Anderson, H. L. Thiophene-Based Dyes for Probing Membranes. *Org. Biomol. Chem.* **2015**, *13*, 3792–3802.

(168)   Abboud, J.-L. M.; Foces-Foces, C.; Notario, R.; Trifonov, R. E.; Volovodenko, A. P.; Ostrovskii, V. A.; Alkorta, I.; Elguero, J. Basicity of N-H- and N-Methyl-1,2,3-Triazoles in the Gas Phase, in Solution, and in the Solid State − An Experimental and Theoretical Study. *Eur. J. Org. Chem.* **2001**, *2001*, 3013–3024.

(169)   Verolet, Q.; Rosspeintner, A.; Soleimanpour, S.; Sakai, N.; Vauthey, E.; Matile, S. Turn-On Sulfide π Donors: An Ultrafast Push for Twisted Mechanophores. *J. Am. Chem. Soc.* **2015**, *137*, 15644–15647.

(170)   Verolet, Q.; Molin, M. D.; Colom, A.; Roux, A.; Guénée, L.; Sakai, N.; Matile, S. Twisted Push-Pull Probes with Turn-On Sulfide Donors. *Helv. Chim. Acta* **2017**, *100*, e1600328.

(171)   Neuhaus, F.; Zobi, F.; Brezesinski, G.; Dal Molin, M.; Matile, S.; Zumbuehl, A. Correlation of Surface Pressure and Hue of Planarizable Push–Pull Chromophores at the Air/Water Interface. *Beilstein J. Org. Chem.* **2017**, *13*, 1099–1105.

(172)   Licari, G.; Beckwith, J. S.; Soleimanpour, S.; Matile, S.; Vauthey, E. Detecting Order and Lateral Pressure at Biomimetic Interfaces Using a Mechanosensitive Second-Harmonic-Generation Probe. *Phys. Chem. Chem. Phys.* **2018**, *20*, 9328–9336.

(173)   Colom, A.; Derivery, E.; Soleimanpour, S.; Tomba, C.; Molin, M. D.; Sakai, N.; González-Gaitán, M.; Matile, S.; Roux, A. A Fluorescent Membrane Tension Probe. *Nat. Chem.* **2018**, *10*, 1118–1125.

(174)   Ho, J. C. S.; Rangamani, P.; Liedberg, B.; Parikh, A. N. Mixing Water, Transducing

Energy, and Shaping Membranes: Autonomously Self-Regulating Giant Vesicles. *Langmuir* **2016**, *32*, 2151–2163.

(175)   Hamada, T.; Kishimoto, Y.; Nagasaki, T.; Takagi, M. Lateral Phase Separation in Tense Membranes. *Soft Matter* **2011**, *7*, 9061.

(176)   Riggi, M.; Niewola-Staszkowska, K.; Chiaruttini, N.; Colom, A.; Kusmider, B.; Mercier, V.; Soleimanpour, S.; Stahl, M.; Matile, S.; Roux, A.; Loewith, R. Decrease in Plasma Membrane Tension Triggers PtdIns(4,5)P$_2$ Phase Separation to Inactivate TORC2. *Nat. Cell Biol.* **2018**, *20*, 1043–1051.

(177)   Strakova, K.; Soleimanpour, S.; Diez-Castellnou, M.; Sakai, N.; Matile, S. Ganglioside-Selective Mechanosensitive Fluorescent Membrane Probes. *Helv. Chim. Acta* **2018**, *101*, e1800019.

(178)   Goujon, A.; Straková, K.; Sakai, N.; Matile, S. Streptavidin Interfacing as a General Strategy to Localize Fluorescent Membrane Tension Probes in Cells. *Chem. Sci.* **2019**, *10*, 310–319.

(179)   Goujon, A.; Colom, A.; Straková, K.; Mercier, V.; Mahecic, D.; Manley, S.; Sakai, N.; Roux, A.; Matile, S. Mechanosensitive Fluorescent Probes to Image Membrane Tension in Mitochondria, Endoplasmic Reticulum, and Lysosomes. *J. Am. Chem. Soc.* **2019**, *141*, 3380–3384.

(180)   Kim, O.-K.; Lehn, J.-M. Solvatochromism of Non-Linear Optical Chromophores Containing the Dithienothiophene Group in Donor-Acceptor Molecules. *Chem. Phys. Lett.* **1996**, *255*, 147–150.

(181)   Kim, O.-K.; Fort, A.; Barzoukas, M.; Blanchard-Desce, M.; Lehn, J.-M. Nonlinear Optical Chromophores Containing Dithienothiophene as a New Type of Electron Relay. *J. Mater. Chem.* **1999**, *9*, 2227–2232.

(182)   Kim, O.-K.; Lee, K.-Sup.; Woo, H. Young.; Kim, K.-S.; He, G. S.; Swiatkiewicz, J.; Prasad, P. N. New Class of Two-Photon-Absorbing Chromophores Based on Dithienothiophene. *Chem. Mater.* **2000**, *12*, 284–286.

(183)   Ortiz, R. P.; Ruiz Delgado, M. C.; Casado, J.; Hernández, V.; Kim, O.-K.; Woo, H. Y.;

López Navarrete, J. T. Electronic Modulation of Dithienothiophene (DTT) as π-Center of D-π-D Chromophores on Optical and Redox Properties: Analysis by UV−Vis−NIR and Raman Spectroscopies Combined with Electrochemistry and Quantum Chemical DFT Calculations. *J. Am. Chem. Soc.* **2004**, *126*, 13363–13376.

(184)   Qin, H.; Wenger, S.; Xu, M.; Gao, F.; Jing, X.; Wang, P.; Zakeeruddin, S. M.; Grätzel, M. An Organic Sensitizer with a Fused Dithienothiophene Unit for Efficient and Stable Dye-Sensitized Solar Cells. *J. Am. Chem. Soc.* **2008**, *130*, 9202–9203.

(185)   Kwon, T.-H.; Armel, V.; Nattestad, A.; MacFarlane, D. R.; Bach, U.; Lind, S. J.; Gordon, K. C.; Tang, W.; Jones, D. J.; Holmes, A. B. Dithienothiophene (DTT)-Based Dyes for Dye-Sensitized Solar Cells: Synthesis of 2,6-Dibromo-DTT. *J. Org. Chem.* **2011**, *76*, 4088–4093.

(186)   Cheng, X.; Liang, M.; Sun, S.; Shi, Y.; Ma, Z.; Sun, Z.; Xue, S. Synthesis and Photovoltaic Properties of Organic Sensitizers Containing Electron-Deficient and Electron-Rich Fused Thiophene for Dye-Sensitized Solar Cells. *Tetrahedron* **2012**, *68*, 5375–5385.

(187)   Shellaiah, M.; Fang, H.-P.; Lin, Y.-L.; Hsu, Y.-C.; Lin, J.-T.; Lin, H.-C. Synthesis of Metal-Free Organic Dyes Containing Tris(Dodecyloxy)Phenyl and Dithienothiophenyl Units and a Study of Their Mesomorphic and Photovoltaic Properties. *Tetrahedron* **2013**, *69*, 2124–2130.

(188)   Marco, A. B.; Andreu, R.; Franco, S.; Garín, J.; Orduna, J.; Villacampa, B.; Alicante, R. Efficient Second-Order Nonlinear Optical Chromophores Based on Dithienothiophene and Thienothiophene Bridges. *Tetrahedron* **2013**, *69*, 3919–3926.

(189)   Akhtaruzzaman, Md.; Menggenbateer; Islam, A.; El-Shafei, A.; Asao, N.; Jin, T.; Han, L.; Alamry, K. A.; Kosa, S. A.; Asiri, A. M.; Yamamoto, Y. Structure–Property Relationship of Different Electron Donors: Novel Organic Sensitizers Based on Fused Dithienothiophene π-Conjugated Linker for High Efficiency Dye-Sensitized Solar Cells. *Tetrahedron* **2013**, *69*, 3444–3450.

(190)   Kumaresan, P.; Liu, Y.-Y.; Vegiraju, S.; Ezhumalai, Y.; Yu, H.-C.; Yau, S. L.; Chen, M.-C.; Lin, T.-C. Synthesis and Characterization of Two-Photon Active Chromophores Based on

Tetrathienoacene (TTA) and Dithienothiophene (DTT). *Chem. Asian J.* **2015**, *10*, 1640–1646.

(191)   Lim, H. C.; Kim, J.-J.; Jang, J.; Hong, J.-I. Effect of the π-Linker on the Performance of Organic Photovoltaic Devices Based on Push–Pull D–π–A Molecules. *New J. Chem.* **2018**, *42*, 11458–11464.

(192)   Arbizzani, C.; Catellani, M.; Mastragostino, M.; Cerroni, M. G. A Spectroelectrochemical Study of Poly(Dithienothiophenes). *J. Electroanal. Chem.* **1997**, *423*, 23–28.

(193)   Osken, I.; Gundogan, A. S.; Tekin, E.; Eroglu, M. S.; Ozturk, T. Fluorene–Dithienothiophene-*S,S*-Dioxide Copolymers. Fine-Tuning for OLED Applications. *Macromolecules* **2013**, *46*, 9202–9210.

(194)   Fang, H.-P.; Wu, Y.-H. Synthesis and Study of Novel Supramolecular Nanocomposites Containing Aryl-Imidazo-Phenanthroline-Based Metallo-Polymers (H-Donors) and Surface-Modified ZnO Nanoparticles (H-Acceptors). *Tetrahedron* **2013**, *69*, 293–301.

(195)   Zhan, X.; Tan, Z.; Domercq, B.; An, Z.; Zhang, X.; Barlow, S.; Li, Y.; Zhu, D.; Kippelen, B.; Marder, S. R. A High-Mobility Electron-Transport Polymer with Broad Absorption and Its Use in Field-Effect Transistors and All-Polymer Solar Cells. *J. Am. Chem. Soc.* **2007**, *129*, 7246–7247.

(196)   Zhan, X.; Tan, Z.; Zhou, E.; Li, Y.; Misra, R.; Grant, A.; Domercq, B.; Zhang, X.-H.; An, Z.; Zhang, X.; Barlow, S.; Kippelen, B.; Marder S. R. Copolymers of Perylene Diimide with Dithienothiophene and Dithienopyrrole as Electron-Transport Materials for All-Polymer Solar Cells and Field-Effect Transistors. *J. Mater. Chem.* **2009**, *19*, 5794–5803.

(197)   Zhang, S.; Wen, Y.; Zhou, W.; Guo, Y.; Ma, L.; Zhao, X.; Zhao, Z.; Barlow, S.; Marder, S. R.; Liu, Y.; Zhan, X. Perylene Diimide Copolymers with Dithienothiophene and Dithienopyrrole: Use in n-Channel and Ambipolar Field-Effect Transistors. *J. Polym. Sci. Part Polym. Chem.* **2013**, *51*, 1550–1558.

(198)   Zhao, X.; Ma, L.; Zhang, L.; Wen, Y.; Chen, J.; Shuai, Z.; Liu, Y.; Zhan, X. An Acetylene-Containing Perylene Diimide Copolymer for High Mobility n-Channel Transistor in Air. *Macromolecules*

2013, *46*, 2152–2158.

(199)   Jang, S.-Y.; Kim, I.-B.; Kim, J.; Khim, D.; Jung, E.; Kang, B.; Lim, B.; Kim, Y.-A.; Jang, Y. H.; Cho, K.; Kim, D.-Y. New Donor–Donor Type Copolymers with Rigid and Coplanar Structures for High-Mobility Organic Field-Effect Transistors. *Chem. Mater.* **2014**, *26*, 6907–6910.

(200)   Luzzati, S.; Basso, M.; Catellani, M.; Brabec, C. J.; Gebeyehu, D.; Sariciftci, N. S. Photo-Induced Electron Transfer from a Dithieno Thiophene-Based Polymer to TiO2. *Thin Solid Films* **2002**, *403–404*, 52–56.

(201)   Catellani, M.; Boselli, B.; Luzzati, S.; Tripodi, C. Dithienothiophene and Dithienothiophene-*S,S*-Dioxide Copolymers for Photovoltaics. *Thin Solid Films* **2002**, *403–404*, 66–70.

(202)   Jackson, N. E.; Savoie, B. M.; Kohlstedt, K. L.; Olvera de la Cruz, M.; Schatz, G. C.; Chen, L. X.; Ratner, M. A. Controlling Conformations of Conjugated Polymers and Small Molecules: The Role of Nonbonding Interactions. *J. Am. Chem. Soc.* **2013**, *135*, 10475–10483.

(203)   Cui, C.; Fan, X.; Zhang, M.; Zhang, J.; Min, J.; Li, Y. A D–A Copolymer of Dithienosilole and a New Acceptor Unit of Naphtho[2,3-*c*]thiophene-4,9-dione for Efficient Polymer Solar Cells. *Chem. Commun.* **2011**, *47*, 11345-11347.

(204)   Huang, J.; Ie, Y.; Karakawa, M.; Saito, M.; Osaka, I.; Aso, Y. Enhanced Photovoltaic Performance of Amorphous Copolymers Based on Dithienosilole and Dioxocycloalkene-Annelated Thiophene. *Chem. Mater.* **2014**, *26*, 6971–6978.

(205)   Guo, X.; Xin, H.; Kim, F. S.; Liyanage, A. D. T.; Jenekhe, S. A.; Watson, M. D. Thieno[3,4-*c*]pyrrole-4,6-dione-Based Donor−Acceptor Conjugated Polymers for Solar Cells. *Macromolecules* **2011**, *44*, 269–277.

(206)   Chu, T.-Y.; Lu, J.; Beaupré, S.; Zhang, Y.; Pouliot, J.-R.; Wakim, S.; Zhou, J.; Leclerc, M.; Li, Z.; Ding, J.; Tao, Y. Bulk Heterojunction Solar Cells Using Thieno[3,4-*c*]pyrrole-4,6-dione and Dithieno[3,2-*b* :2′,3′-*d*]silole Copolymer with a Power Conversion Efficiency of 7.3%. *J. Am. Chem. Soc.* **2011**, *133*, 4250–4253.

(207)   Takacs, C. J.; Sun, Y.; Welch, G. C.; Perez, L. A.; Liu, X.; Wen, W.; Bazan, G. C.; Heeger, A. J. Solar Cell Efficiency, Self-Assembly, and Dipole–Dipole Interactions of Isomorphic Narrow-Band-Gap Molecules. *J. Am. Chem. Soc.* **2012**, *134*, 16597–16606.

(208)   Welch, G. C.; Perez, L. A.; Hoven, C. V.; Zhang, Y.; Dang, X.-D.; Sharenko, A.; Toney, M. F.; Kramer, E. J.; Nguyen, T.-Q.; Bazan, G. C. A Modular Molecular Framework for Utility in Small-Molecule Solution-Processed Organic Photovoltaic Devices. *J. Mater. Chem.* **2011**, *21*, 12700–12709.

(209)   Welch, G. C.; Bakus, R. C.; Teat, S. J.; Bazan, G. C. Impact of Regiochemistry and Isoelectronic Bridgehead Substitution on the Molecular Shape and Bulk Organization of Narrow Bandgap Chromophores. *J. Am. Chem. Soc.* **2013**, *135*, 2298–2305.

(210)   Gupta, V.; Lai, L. F.; Datt, R.; Chand, S.; Heeger, A. J.; Bazan, G. C.; Singh, S. P. Dithienogermole-Based Solution-Processed Molecular Solar Cells with Efficiency over 9%. *Chem. Commun.* **2016**, *52*, 8596–8599.

(211)   Ni, W.; Li, M.; Liu, F.; Wan, X.; Feng, H.; Kan, B.; Zhang, Q.; Zhang, H.; Chen, Y. Dithienosilole-Based Small-Molecule Organic Solar Cells with an Efficiency over 8%: Investigation of the Relationship between the Molecular Structure and Photovoltaic Performance. *Chem. Mater.* **2015**, *27*, 6077–6084.

(212)   Polander, L. E.; Tiwari, S. P.; Pandey, L.; Seifried, B. M.; Zhang, Q.; Barlow, S.; Risko, C.; Brédas, J.-L.; Kippelen, B.; Marder, S. R. Solution-Processed Molecular Bis(Naphthalene Diimide) Derivatives with High Electron Mobility. *Chem. Mater.* **2011**, *23*, 3408–3410.

(213)   Zhang, J.; Singh, S.; Hwang, D. K.; Barlow, S.; Kippelen, B.; Marder, S. R. 2-Bromo Perylene Diimide: Synthesis Using C–H Activation and Use in the Synthesis of Bis(Perylene Diimide)–Donor Electron-Transport Materials. *J. Mater. Chem. C* **2013**, *1*, 5093–5100.

(214)   Hunziker, C.; Zhan, X.; Losio, P. A.; Figi, H.; Kwon, O.-P.; Barlow, S.; Günter, P.; Marder, S. R. Highly Ordered Thin Films of a Bis(dithienothiophene) Derivative. *J. Mater. Chem.* **2007**, *17*, 4972-4979.

(215)   Mazzeo, M.; Vitale, V.; Della Sala, F.; Anni, M.; Barbarella, G.; Favaretto, L.; Sotgiu, G.; Cingolani, R.; Gigli, G. Bright White Organic Light-Emitting Devices from a Single Active Molecular Material. *Adv. Mater.* **2005**, *17*, 34–39.

(216)   Cicoira, F.; Santato, C.; Melucci, M.; Favaretto, L.; Gazzano, M.; Muccini, M.; Barbarella, G. Organic Light-Emitting Transistors Based on Solution-Cast and Vacuum-Sublimed Films of a Rigid Core Thiophene Oligomer. *Adv. Mater.* **2006**, *18*, 169–174.

(217)   Palamà, I.; Di Maria, F.; Viola, I.; Fabiano, E.; Gigli, G.; Bettini, C.; Barbarella, G. Live-Cell-Permeant Thiophene Fluorophores and Cell-Mediated Formation of Fluorescent Fibrils. *J. Am. Chem. Soc.* **2011**, *133*, 17777–17785.

(218)   Viola, I.; Palamà, I. E.; Coluccia, A. M. L.; Biasiucci, M.; Dozza, B.; Lucarelli, E.; Di Maria, F.; Barbarella, G.; Gigli, G. Physiological Formation of Fluorescent and Conductive Protein Microfibers in Live Fibroblasts upon Spontaneous Uptake of Biocompatible Fluorophores. *Integr. Biol.* **2013**, *5*, 1057–1066.

(219)   Palamà, I. E.; Di Maria, F.; D'Amone, S.; Barbarella, G.; Gigli, G. Biocompatible and Biodegradable Fluorescent Microfibers Physiologically Secreted by Live Cells upon Spontaneous Uptake of Thiophene Fluorophore. *J. Mater. Chem. B* **2015**, *3*, 151–158.

(220)   Maria, F. D.; Zangoli, M.; Gazzano, M.; Fabiano, E.; Gentili, D.; Zanelli, A.; Fermi, A.; Bergamini, G.; Bonifazi, D.; Perinot, A.; Caironi, M.; Mazarro, R.; Morandi, V.; Gigli, G.; Liscio, A.; Barbarella, G. Controlling the Functional Properties of Oligothiophene Crystalline Nano/Microfibers via Tailoring of the Self-Assembling Molecular Precursors. *Adv. Funct. Mater.* **2018**, *28*, 1801946.

(221)   Kim, K. H.; Chi, Z.; Cho, M. J.; Jin, J.-I.; Cho, M. Y.; Kim, S. J.; Joo, J.; Choi, D. H. Soluble Star-Shaped Molecules Based on Thiophene Derivatives as Organic Semiconductors for Field-Effect Transistor Applications. *Chem. Mater.* **2007**, *19*, 4925–4932.

(222)   Irie, M.; Fukaminato, T.; Matsuda, K.; Kobatake, S. Photochromism of Diarylethene Molecules and Crystals: Memories, Switches, and Actuators. *Chem. Rev.* **2014**, *114*, 12174–12277.

(223)   Wang, H.; Lin, H.; Xu, W.; Zhu, D. Nonsymmetrical Dithienylethenes Bearing Dithieno[3,2-*b*:2′,3′-*d*]thiophene Units with Photochromic Performance in the Crystalline Phase. *Chem. Eur. J.* **2013**, *19*, 3366–3373.

(224)   Wang, H.; Xu, W.; Zhu, D. Photochromism of Diarylethenes Containing Dithieno[3,2-*b*:2′,3′-*d*]thiophene. *Dyes Pigments* **2013**, *97*, 303–310.

(225)   Lin, H.; Xu, W.; Zhu, D. 1,2-Bis(3,5-dimethyl-dithieno[3,2-*b*:2′,3′-*d*]thiophene-2-yl) Perfluorocyclopentene: Synthesis and Photochromic Reaction in Solution and LB Films. *J. Mater. Chem.* **2010**, *20*, 884–890.

(226)   Cha, W.-Y.; Kim, T.; Ghosh, A.; Zhang, Z.; Ke, X.-S.; Ali, R.; Lynch, V. M.; Jung, J.; Kim, W.; Lee, S.; Fukuzumi, S.; Park, J. S.; Sessler, J. L.; Chandrashekar, T. K.; Kim, D. Bicyclic Baird-Type Aromaticity. *Nat. Chem.* **2017**, *9*, 1243–1248.

(227)   Sarma, T.; Kim, G.; Sen, S.; Cha, W.-Y.; Duan, Z.; Moore, M. D.; Lynch, V. M.; Zhang, Z.; Kim, D.; Sessler, J. L. Proton-Coupled Redox Switching in an Annulated π-Extended Core-Modified Octaphyrin. *J. Am. Chem. Soc.* **2018**, *140*, 12111–12119.

(228)   Inoue, R.; Hasegawa, M.; Nishinaga, T.; Yoza, K.; Mazaki, Y. Efficient Synthesis, Structure, and Complexation Studies of Electron-Donating Thiacalix[n]dithienothiophene. *Angew. Chem. Int. Ed.* **2015**, *54*, 2734–2738.